Nature Communications

https://doi.org/10.1038/s41467-026-69602-x

Article in Press

Pyrimidinergic calcium signaling links tubular metabolism to fibrosis in kidney disease

Received: 3 March 2025

Accepted: 5 February 2026

Cite this article as: Figurek, A., Jankovic, N., Kollar, S. *et al.* Pyrimidinergic calcium signaling links tubular metabolism to fibrosis in kidney disease. *Nat Commun* (2026). https://doi.org/10.1038/s41467-026-69602-x

Andreja Figurek, Nevena Jankovic, Sarah Kollar, Monika Kaminska, Imene Sakhi, Anna Rinaldi, Pietro E. Cippà, Bernard Robaye & Andrew M. Hall

Pyrimidinergic calcium signaling links tubular metabolism to fibrosis in kidney disease

Andreja Figurek[1], Nevena Jankovic[1], Sarah Kollar[1], Monika Kaminska[1], Imene Sakhi[1], Anna Rinaldi[2,3], Pietro E Cippà[2,3], Bernard Robaye[4], Andrew M Hall[1,5,6].

Affiliations: [1]Institute of Anatomy, University of Zurich, Zurich, Switzerland. [2]Laboratories for Translational Research, Ente Ospedaliero Cantonale, Bellinzona, Switzerland. [3]Department of Medicine, Division of Nephrology, Ente Ospedaliero Cantonale, Lugano, Switzerland. [4]IRIBHM, University of Brussels, Brussels, Belgium. [5]Department of Nephrology, University Hospital Zurich, Zurich, Switzerland. [6]Zurich Kidney Center, Zurich, Switzerland.

Contact:
andrew.hall@uzh.ch

Address for submission correspondence:
Andrew Hall MD PhD
Institute of Anatomy
University of Zurich
Winterthurerstrasse 190
8057 Zurich
Switzerland
Email: andrew.hall@uzh.ch
Tel: +41 (0)44 635 52 25
Fax: +41 (0)44 635 57 02

Word count: 8930.

Running title: Pyrimidinergic signaling in kidney disease

Keywords: Kidney disease, pyrimidine, tubule, fibrosis, calcium, P2Y6, UDP.

Abstract

Chronic kidney disease (CKD) is a major global health problem, with substantial associated morbidity and mortality. Fibrosis is the final common pathway of organ damage in CKD, so understanding how this arises during kidney injury is critical for building a holistic picture of the pathogenesis. Here, using gene expression data, intravital microscopy in mice and realistic cell models, we uncover evidence of a signaling pathway linking tubular pyrimidine metabolism and injury-evoked extracellular uridine diphosphate (UDP) release to activation of the P2Y6 receptor (P2Y6R) in surrounding fibroblasts. We show that P2Y6R activation triggers intracellular calcium rises, which stimulate fibroblast proliferation, migration, and conversion towards a myofibroblast phenotype. Conversely, genetic knockout or pharmacological blockade of the P2Y6R reduces fibrosis in mice with CKD. Thus, we reveal that pyrimidinergic calcium signaling couples fibroblast responses to changes in tubular metabolism in disease states, and represents a potential new target for therapeutic intervention.

Introduction

Chronic kidney disease (CKD) affects 1 in 10 people and can lead to kidney failure, which has major adverse effects on health systems, economies and the environment[1,2]. CKD is a strong independent risk factor for cardiovascular disease and is predicted to become the 4th leading cause of death of 2040[3], so there is a pressing need to unravel the pathophysiology of CKD and develop new therapies.

The proximal tubule is the workhorse of the kidney, responsible for reabsorbing most of the glomerular filtrate. Metabolism in the proximal tubule is complex and closely entwined with solute transport[4], and can change substantially in disease states[5–7]. Interstitial fibroblasts surround proximal tubules with long processes[8]; activation of these cells and transformation to a myofibroblast phenotype is a critical step in CKD progression, which leads to secretion of collagen and other extracellular matrix proteins, and ultimately the replacement of healthy parenchyma[7,9–12]. Extracellular sensing of metabolite release could provide a possible mechanism to couple fibroblast responses with alterations in tubular activity.

Pyrimidines have multiple important roles in cell biology and can be generated by *de novo* synthesis or salvage pathways, with the latter generally predominating in differentiated cells[13]. Here, using gene expression analysis we find evidence that pyrimidine metabolism is active in proximal tubules, and when injured they upregulate a key enzyme in the pyrimidine salvage pathway. Moreover, induction of damage in cultured proximal tubular cells causes UDP release into the extracellular environment. Furthermore, we show that the target receptor for UDP (the P2Y6 receptor [P2Y6R]) is present in neighboring fibroblasts and that its expression increases in disease models. Thus, pyrimidinergic signaling represents a plausible pathway for tubulo-interstitial crosstalk in CKD.

Results

Pyrimidine metabolism is highly active in proximal tubules, which release UDP when injured

We began by interrogating a single cell sequencing dataset derived from mice with renal ischemia-reperfusion injury[14–16], and identified a high expression of genes involved in pyrimidine metabolism in proximal tubules (Figure 1 a, Supplementary figure 1). Moreover, both healthy tubules and emerging new and injured cell populations expressed *cda* (Figure 1 b), which encodes the key pyrimidine salvage pathway enzyme cytidine deaminase (CDA) that converts cytidine to uridine to maintain the cellular UDP pool[17]. Furthermore, antibody staining of fixed kidneys in two mouse models of CKD - unilateral ureteric obstruction (UUO) and folic acid nephropathy (FAN) - revealed a dramatic increase in abundance of CDA in aquaporin-1 positive proximal tubules, with evidence of activation of surrounding fibroblasts (increased expression of alpha smooth muscle actin [αSMA]) (Figure 1 c and Supplementary figure 2).

Expression of *cda* was also detected in human proximal tubule-derived cells (HK-2) in culture and increased significantly after induction of injury with cisplatin or folic acid (Figure 1 d). Crucially, this was accompanied by a rise in extracellular UDP concentration, denoting release from cells (Figure 1 e). However, due to technical constraints, we were not able to assess UDP release from tubules *in vivo*.

Expression of the P2Y6R increases in kidney fibroblasts in disease states

These data suggest that injured proximal tubular cells produce and release UDP, which is the endogenous ligand for the P2Y6R. We therefore analyzed the renal expression of this receptor in single cell databases and found that it is not only expressed in pdgfrb positive stromal cells, but that its expression increases in models of CKD caused by ischemia-reperfusion injury[14–16] or glomerulopathy (POD-ATTAC)[18] (Figure 2 a, b and Supplementary figures 3 and 4). Although significant, changes in P2Y6R expression in these datasets were quite small; however, much larger increases were confirmed at the whole kidney level by RT-qPCR in mice with UUO or FAN, with global P2Y6R knockout (KO) mice used as a control[19] (Figure 2 c, d).

Activation of the P2Y6R can induce calcium release within cells via phospholipase C[20]. To investigate the effects of P2Y6R stimulation on calcium signals in kidney tissue we used freshly cut slices from the kidneys of transgenic mice expressing the fluorescent calcium reporter GCaMP6s[21], and observed that application of either UDP or a synthetic agonist (MRS2957)[22] induced calcium rises in interstitial cells (Supplementary figure 5), which were inhibited by the non-specific purinergic blocker suramin or a specific P2Y6 antagonist (MRS2578) (Figure 2 e-g). In addition, both agonists stimulated increases in intracellular calcium in cultured rat renal fibroblasts transfected with GCaMP6s (NRK-49F), which appeared initially in cell processes before propagating towards the cell body (Figure 2 h-k).

In summary, these data indicate a high level of pyrimidinergic signaling machinery in the tubulointerstitial compartment, which potentially ramps up in disease states.

Activation of the P2Y6 receptor stimulates proliferation, migration and pro-fibrotic gene expression in renal fibroblasts

To investigate the functional consequences of activating the P2Y6R in renal fibroblasts, we incubated NRK-49F cells with a P2Y6R agonist (MRS2957) for 24 hours and found that this significantly increased cell proliferation and migration compared to controls (Figure 3 a-b). Blockade of the P2Y6R with an antagonist (MRS2578) abolished these effects, as did chelation of intracellular calcium with BAPTA-AM ((1,2-bis(o-aminophenoxy) ethane-N,N,N′,N′-tetraacetic acid) (Figure 3 c-d), indicating a dependence on calcium release. In addition, P2Y6R activation increased expression of genes encoding the proliferation marker MKI67 and the pro-fibrotic markers PDGFRβ, αSMA, fibronectin, vimentin, and collagen 1 (Figure 3 e). Finally, increased abundance of fibronectin and vimentin was confirmed at protein level after 72 hours with antibody staining (Figure 3 f, g). In contrast, knocking down the P2Y6R in NRK-49F cells with siRNA blunted agonist effects on cell proliferation and activation of fibrosis markers (Supplementary figure 6).

Fibroblasts in mouse kidneys display spontaneous calcium signals in processes surrounding tubules

Having identified that injured tubules release UDP and that this can induce calcium rises in renal fibroblasts *in vitro* or *ex vivo*, we proceeded to investigate the nature of fibroblast calcium signals *in vivo*, by performing intravital multiphoton microscopy in GCaMP6s expressing mice. To confirm expression of GCaMP6s in fibroblasts, we used antibody staining in fixed tissue for the well-established marker Platelet Derived Growth Factor Receptor beta (PDGFRβ), which labeled a population of interstitial cells distinct from MHC class II positive immune cells (Supplementary figure 7). During these experiments, we observed spontaneous slow calcium transients arising in proximal tubular cells, as previously reported[21]. In addition, we noted spontaneous calcium rises in interstitial cells surrounding tubules and exhibiting a fibroblast morphology (Figure 4 a-c). To confirm their identity, we marked the region of live imaging, fixed and sliced tissue and retrospectively stained it for PDGFRβ. Visualization of calcium traces from PDGFRβ positive cells revealed a different dynamic from proximal tubules. In contrast to periodic, discrete transients, fibroblast calcium signals were more frequent and noisier (Figure 4 d-e).

To elucidate the spatiotemporal pattern of intracellular calcium signals in renal fibroblasts in more detail, we imaged them in freshly cut slices of mouse kidney tissue, which allowed us to visualize cells with multiple processes contained within the same field of view (Figure 4 f-i). From this we could ascertain that calcium signals in fibroblasts arose in processes, before propagating across cells (Figure 4 j and Supplementary movie 1).

Taken together, these findings indicate that calcium signals in renal fibroblasts comprise (relatively) fast and irregular transients originating in processes wrapping around tubules, which raises the possibility that they could triggered by signaling factors emanating from the latter.

Calcium activity in kidney fibroblasts increases in mouse models of tubular injury and kidney fibrosis

Next, we wanted to know if tubular injury stimulates calcium signaling in fibroblasts. To investigate this, we injected GCaMP6s expressing mice with the tubular toxin cisplatin (20 mg/kg, intraperitoneal), according to an established protocol[21]. After 72 hours, we observed that calcium transients were reduced in frequency in proximal tubules, denoting epithelial damage (Figure 5 b, c, e). Conversely, calcium activity in surrounding fibroblasts was significantly increased, indicating a signaling response (Figure 5 d and Supplementary movie 2).

To explore the nature of calcium signaling in renal fibrosis during CKD, we used the UUO model. After 7 days, filtration and tubular uptake of a small fluorescently labeled dextran was severely impaired in UUO mice, signifying a considerable defect in kidney function, and calcium transients were almost completely abolished in proximal tubules (Figure 5 f, g, i). In contrast, calcium signaling was increased in fibroblasts (Figure 5 h and Supplementary movie 3), and this was associated with proliferation of PDGFRβ positive cells and elevated expression of αSMA, indicating activation and conversion to a myofibroblast phenotype (Figure 5 j-m).

Knockout or inhibition of the P2Y6 receptor decreases kidney fibrosis in ureteric obstruction

Having uncovered evidence of a signaling pathway involving UDP activation of the P2Y6R in renal fibroblasts, we wanted to know if disrupting this would impact on fibrosis. We therefore used global P2Y6R KO mice[19], and subjected them to UUO for 7 days. In comparison to wildtype littermates, obstructed kidneys in KO mice displayed less fibroblast proliferation, lower expression of fibronectin, αSMA, and collagen 1, fewer infiltrating macrophages, and decreased total area of fibrosis (measured using Sirius red staining) (Figure 6).

Next, to investigate the consequences of blocking the P2Y6R with a pharmacological approach, we performed 7-day UUO experiments in wildtype mice treated with daily injections of either a P2Y6R

antagonist (MRS2578) or placebo, and found that the former produced similar beneficial effects on renal fibrosis to P2Y6 KO (Figure 7). Moreover, P2Y6R blockade also decreased calcium signaling in fibroblasts in GCaMP6s expressing mice subjected to UUO (Supplementary figure 8).

Knockout or inhibition of the P2Y6 receptor decreases kidney fibrosis in folic acid nephropathy

To validate findings with the UUO model, we repeated experiments in FAN and observed that kidneys in KO animals displayed lower fibroblast proliferation and expression of pro-fibrotic markers, decreased macrophage infiltration, and a smaller total area of fibrosis (Figure 8 a, b, c). Moreover, blood urea and creatinine levels were significantly lower in KO mice, denoting an improvement in kidney excretory function (Figure 8 d).

Finally, we performed folic acid experiments in wildtype mice treated either with a P2Y6R antagonist (MRS2578) or vehicle and observed that the former were protected against renal fibrosis (Figure 9 a, b, c). Mean urea and creatinine levels were lower in antagonist treated mice, but differences between groups were not statistically significant, due to a high variability in values within treatment groups (Figure 9 d).

To conclude, these results demonstrate that blocking the UDP-P2Y6R signaling axis is protective against the development of renal fibrosis in mice with CKD.

Discussion

CKD is a global epidemic and there is an urgent need to elucidate mechanisms that translate episodic tubular injury into irreversible fibrosis. In this study, we deployed gene expression analysis, cutting-edge intravital imaging techniques and other orthogonal approaches to investigate tubulointerstitial interactions within functioning kidneys and made three important discoveries (Figure 10). First, we identified evidence that pyrimidine metabolism is highly active in proximal tubules, and that P2Y6R activation induces calcium signals, proliferation and pro-fibrotic responses in neighboring fibroblasts.

Second, we observed that renal fibroblasts display spontaneous calcium transients that arise in processes wrapping around tubules, and that this activity increases dramatically in response to tubular injury, indicating a signaling response. Finally, we demonstrated that depleting or blocking the P2Y6R reduced fibrosis in disease models, illustrating the potential relevance of this pathway in CKD progression.

Changes in tubular metabolism are emerging as a central feature of CKD, but how these are linked to fibrotic responses is still not well understood[7]. Our gene expression analysis suggests a preponderance of pyrimidine metabolism in proximal tubules. Interestingly, a recent study reported that filtered pyrimidines are reabsorbed in this nephron segment, and that knockout of the responsible apical transporter induces urinary loss of pyrimidines and other metabolites[23]. We do not know why the key enzyme CDA is upregulated in kidney injury, but speculative reasons could include a greater demand for pyrimidines in proliferating epithelial cells undergoing a reparative process. Of note, renal fibroblasts highly express ectonucleotidases[8], providing further evidence that they are exposed to extracellular nucleotides. However, due to technical constraints we could only detect UDP release from cultured cells; whether this occurs from proximal tubules or other sources *in vivo* remains to be determined.

Although P2Y6R inhibition was protective in our experiments, it did not completely prevent fibrosis. Other pro-fibrotic signaling molecules might also activate calcium signals in renal fibroblasts; for example, a previous imaging study showed that PDGF inhibition blunts calcium rises and fibroblast migration in response to laser-induced injury[24], while blocking the Transient Receptor Potential Canonical 3 (TRPC3) calcium channel decreases fibrosis in UUO models[25]. Therefore, it will be interesting to explore whether targeting these pathways and the P2Y6R produces synergistic effects. However, while fibroblast calcium signaling was markedly increased in disease states, we observed some spontaneous activity even under physiological conditions. Thus, calcium may be important for normal housekeeping functions, such as maintenance of the actin cytoskeleton, so complete abolition may be undesirable.

The discovery of P2Y6R signaling in kidney disease adds to the growing literature highlighting this pathway in other organs and diseases, including pressure overload cardiac fibrosis[26], lung inflammation[19], brain diseases[27] and the vasculature in hypertension[28]. Moreover, a very recent study identified a protective effect against atherosclerosis in mice with CKD[29]. Importantly, the P2Y6R is an attractive target for therapies, since KO mice do not display a phenotype at baseline, but renal expression is increased in CKD.

There are some potential limitations to our study. First, the P2Y6R deficient mouse model we used is a global KO, which is not specific to kidney fibroblasts, meaning that some effects could be mediated via other cell types. Expression of the receptor was also detected at RNA level in immune cells, which might amplify the anti-fibrotic effects of P2Y6R blockade and this possibility should be further investigated. Second, as mentioned, we were not able to assess UDP release in the kidney *in vivo*. Third, although we identified that P2Y6R blockade is protective against fibrosis, we do not yet know whether this will translate into long term benefits in kidney function. Fourth, we cannot be sure that the same signaling pathways are active in humans, although we note a single cell sequencing study that identified upregulation of calcium dependent genes in activated human fibroblasts[30].

In summary, we show that pyrimidinergic calcium signaling is an important regulator of fibroblast activity in the kidney in response to metabolic and microenvironmental changes, and this discovery may facilitate new strategies to modify the behavior of these cells in a variety of different disease states.

Methods

Reagents

Unless stated otherwise, all reagents were purchased from Sigma Aldrich.

Dyes

Dextran Alexa 647 (D22914, Thermo Fisher Scientific) was purchased from the manufacturer.

Cell culture

Normal rat kidney fibroblasts (NRK-49F, CRL-1570, ATCC) were cultured at 37°C in a 5% CO2 humidified atmosphere in Dulbecco's Modified Eagle's Medium (DMEM) containing 5% fetal bovine serum and 1% penicillin/streptomycin. Human cortical proximal tubular cells (HK-2, CRL-2190, ATCC) were cultured in DMEM/F12 media supplemented with REGM Renal Epithelial Cell Growth Medium BulletKit (Lonza), 1% L-Glutamine and 1% PenStrep at 37°C in a 5% CO2 humidified atmosphere.

Cisplatin and folic acid cell models

HK-2 cells were seeded as previously described for both cisplatin and folic acid treatments[31]. Briefly, at 80% confluency cells were washed with PBS and treated with 20 µM cisplatin and NaCl as well as 1mM folic acid and $NaHCO_3$ in supplement-free DMEM/F12 media. For cisplatin experiments, the cells were incubated for 24-48h. For folic acid experiments, the cells were incubated for 72h. Extracellular UDP was quantified with AffiASSAY MicroMolar UDP assay kit (AFG-PRF-266, AffiGEN), by following manufacturer's protocol. Fluorescence was detected on a microplate reader (Cytation 5, BioTek), and UDP concentrations were quantified by using a standard UDP curve.

Fibroblast proliferation experiments

NRK-49F cells were grown in 96-well plates (655087, Greiner) adjusted for fluorescence image quality for 72h in culturing medium. The effect of P2Y6R activation on fibroblast proliferation was examined by adding either 50 µM UDP or 5 µM P2Y6 specific agonist (MRS2957, Cat. No. 4260, Tocris) to serum-free medium for 24h. Bonding and removal of intracellular calcium ions was achieved by incubation with 20 µM calcium chelator 1,2-bis(o-aminophenoxy) ethane-N,N,N',N'-tetraacetic acid (BAPTA-AM, LuBioScience GmbH) for 30 min at 37°C in a 5% CO2 humidified atmosphere. P2Y6R inhibition was achieved by adding 1 µM specific P2Y6R antagonist (MRS2578, Cat. No. 2146, Tocris) to medium containing a P2Y6 receptor agonist (MRS2957). After treatment, NRK-49F cells were washed with pre-warmed (37°C) PBS before being fixed with pre-warmed 4% PFA prepared in PBS for 10 minutes. Fixed

cells were washed with PBS several times and stained with a blue, fluorescent nuclear stain (Hoechst 33342, Sigma). Thereafter, cell number was counted using a widefield fluorescence microscope and fully automated high-content imaging system (IN Cell Analyzer 2500 HS, GE).

Fibroblast migration analysis (in vitro scratch assay)

The effect of P2Y6R activation on fibroblast migration was investigated by a well-established scratch assay[32]. NRK-49F cells were grown in a 12-well plate until confluency, followed by scraping the cell monolayer with a p200 pipet tip in a straight line. The debris was washed with PBS and cells were further incubated in serum-free medium for 24h containing either 50 µM UDP or 5 µM P2Y6R specific agonist (MRS2957). Images were captured at 0h and 24h with Personal AUtomated Lab Assistant PAULA Cell imager (Leica Microsystems).

Analysis of pro-fibrotic protein expression in fibroblasts

NRK-49F cells were grown in 8-well removable chamber slides for immunofluorescence (80841-IBI, Ibidi) for 72h. Subsequently, cells were incubated for another 72h in serum-free medium containing 10 µM P2Y6R specific agonist (MRS2957). After treatment, NRK-49F cells were washed with pre-warmed (37°C) PBS before being fixed with pre-warmed 4% PFA prepared in PBS for 10 minutes. Fixed cells were washed with PBS several times, and permeabilized for 5 minutes with 0.1% TritonX–100 in prepared in PBS at room temperature. After washing with PBS, cells were blocked at room temperature for 30 minutes with 10% donkey and/or goat serum prepared in 1% BSA in PBS. Cells were incubated with following primary antibodies: mouse vimentin (a kind gift from Prof. Johannes Loffing, University of Zurich, 1:50), and rabbit fibronectin (Sigma, F3648, 1:150) overnight at 4°C. On the following day, cells were incubated at room temperature for 2 hours with suitable secondary antibodies: donkey anti-rabbit-AF647 (711-606-152, Jackson ImmunoResearch Europe Ltd, 1:100) and goat anti-mouse-AF568 (A-11004, Thermo Fisher Scientific, 1:100). Imaging was performed on an inverted confocal laser scanning microscope ZEISS LSM 980 Airyscan by using a LD LCI Plan-Apochromat 25x/0.8 silicon-oil objective.

Live cell imaging of calcium signals in cultured fibroblasts

NRK-49F cells were grown in 8-well chamber slides for 72h. Thereafter, transfection with GCaMP6s plasmid (pGP-CMV-GCaMP6s, #40753, Addgene) followed. After 48h cells were perfused with 10 μM P2Y6R agonist (MRS2957) and changes in fluorescence intensity were detected by an inverted confocal laser scanning microscope ZEISS LSM 980 Airyscan by using a LD LCI Plan-Apochromat 25x/0.8 water objective. GCaMP6s signal was imaged at 488 nm and images were recorded every 1.40 seconds.

P2Y6 receptor knock-down in fibroblasts

The silencing of the receptor was performed by transfecting wildtype NRK-49F cells with Dicer-substrate short interfering RNAs (DsiRNAs) targeting P2RY6 (TriFECTa RNAi Kit; IDT Technology) using the Lipofectamine™ RNAiMAX Transfection Reagent (Thermo Fisher Scientific). Briefly, for RT-qPCR experiments, $5x10^5$ cells were transfected according to manufacturer's protocol using 10 nm of P2RY6 DsiRNA and scramble guide as control for 48h. The DsiRNA effect was assessed using RT-qPCR. Sequence of DsiRNA is listed in Supplementary Table S1. The same protocols used for fibroblast proliferation and pro-fibrotic marker expression in wildtype NRK-49F cells were repeated in P2RY6-silenced NRK-49F fibroblasts (NRK-49F^{P2RY6KD}). The effect of P2RY6 knock-down on fibroblast proliferation was assessed after incubation of NRK-49F^{P2RY6KD} for 24h and on pro-fibrotic markers expression for 72h with 10μM P2Y6 receptor agonist (during the project MRS2957 was discontinued by the manufacturer, so in these experiments MRS2693 (Cat. No. 2502, Tocris) was used as a replacement). P2Y6R expression was detected by P2Y6-FITC antibody (Tresars, 1:100).

RNA extraction, cDNA reverse transcription and real time quantitative PCR (RT-qPCR) in cell lines

RNA was extracted, according to the manufacturers protocol, using the miRNeasy Tissue/Cells Advanced Mini Kit (Qiagen). RNA concentration was determined with NanoDrop™ One (Thermo Fisher Scientific) and reverse transcribed using the High-Capacity cDNA Reverse Transcription Kit (Applied Biosystems) according to the manufacturer's protocol. 500nM of both the sense and anti-sense primers were added

to the PowerUP SYBR Green Master Mix (Applied Biosystems). RT-qPCR was performed using a LightCycler 480 system (Roche). For quantification, the relative change of target genes was calculated over that of the housekeeping gene (GAPDH) using the $2^{-\Delta\Delta CT}$ formula[33]. Specific primers were designed for rat (P2RY6, FN1, VIM, COL1A1, ACTA2, PDGFRB, MKI67 and GAPDH) and human targets (NGAL, KIM1, CDA and GAPDH) and are listed in Supplementary Table S2.

Animals

C57BL6 mice

Experiments were performed on 8- to 15-week-old male C57BL mice (supplied by Janvier), in accordance with the regulations of the Zurich cantonal veterinary office (License No. ZH021/2015 and License No. ZH140/2023). Mice were euthanized 7 days following UUO or 14 days following folic acid nephropathy.

GCaMP6s mice

GCaMP6s mice were created by breeding Ai96(RCL-GCaMP6s)[34] JAX stock #024106) with CMV-Cre mice[35] (JAX stock #006054). GCaMP6s^{+}/CMV-Cre^{+} (GCaMP6s) mice are characterized and described previously[21]. Experiments were performed on 8- to 23-week-old male and female GCaMP6s mice, in accordance with the regulations of the Zurich cantonal veterinary office (License No. ZH021/2015 and License No. ZH194/16). Mice were euthanized 3 days after inducing cisplatin nephrotoxicity or 7 days following UUO.

P2Y6 receptor knockout mice

An established mouse line with a global, constitutive depletion of the P2y6r on a C57Bl6 background was generated in IRIBHM (University of Brussels, Belgium), characterized, and described previously[36]. Experiments in these mice were conducted according to the Ethic Committee of Animal Well-Being in Brussels, license number 25GOSIRIBHM. Experiments were performed on 8- to 15-week-old male KO mice

and their wild-type littermates. Mice were euthanized 7 days following UUO or 14 days following folic acid nephropathy.

RNA extraction, cDNA reverse transcription and real time quantitative PCR (RT-qPCR) in mouse kidney

Kidneys were homogenized into 1 ml of Tri Reagent® (Invitrogen). Total RNAs were isolated according to the manufacturer's instructions. After a 30 min DNAse (Thermofisher Scientific) treatment, a reverse transcription of 1µg total RNA was performed using RevertAid H Minus First Strand cDNA Synthesis Kit (Thermofisher Scientific) using random hexamers. Quantitative RT-PCR was performed with iTaq™ Universal SYBR® Green Supermix (Bio-Rad Laboratories) according to the manufacturer's instructions on the iCycler C1000 Real-Time PCR Detection System (Bio-Rad Laboratories). Primers sequences were listed in table Supplementary table S2. All PCRs were performed in duplicate and normalized mRNA expressions were calculated by the $2^{\Delta Cq}$ method using HPRT and RPL32 as internal references: normalized expression=$2^{(CqHPRT+CqRPL32)/2)-CqP2RY6}$.

Imaging of freshly cut kidney slices

Mice were anesthetized with intra-peritoneal injection of ketamine (170 mg/kg) and xylazine (10 mg/kg) and kidneys were harvested. After the kidney capsule was removed, the kidney was mounted and cut with a vibratome (Microm HM 650 V, Thermo Scientific, Waltham, Massachusetts, USA) into 280 µm thick longitudinal sections. The slices were maintained until imaging at 4°C in a physiological buffer containing (in mM): 118 NaCl, 4.7 KCl, 1.2 KH_2PO_4, 1.8 $CaCl_2$, 1.44 $MgSO_4$, 5 glucose, 10 $NaHCO_3$, 10 HEPES, 5 sodium pyruvate, 2.5 sodium butyrate and 2.5 sodium lactate, adjusted to pH 7.4 and gassed with carbogen (95% O_2 / 5% CO_2). Thereafter, slices were placed into a heated chamber at 37 °C (Warner Instruments, Hamden, Connecticut, USA) filled with gassed slice buffer for live imaging with continuous perfusion. For live imaging of kidney medullary slices 50 µM UDP, 50 µM suramin, 10 µM MRS2975 (Tocris) and 10 µM MRS2578 (Tocris) were dissolved in physiological buffer. Video recordings were performed with a Multiphoton - Leica SP8 DIVE FALCON supplied with a Harmonic Compound Infrared Apochromatic L (HC

IRAPO L) 25x/1.0 W motCORR objective and an Insigth DS+ Dual (680-1300 nm & 1041nm) ultrafast Near-Infrared (NIR) laser system. GCaMP6s was excited at 950 nm and visualized at 500-550 nm. GCaMP6s signal was captured every 0.43 seconds. After imaging, the area imaged was marked with a laser to enable later recognition and slices were fixed in 4% PFA for immunofluorescence staining.

Intravital imaging

Following induction of general anesthesia with inhaled isoflurane (1.5 – 5%) and oxygen (600ml/min), the internal jugular vein was cannulated to permit intravenous injections of reagents and dyes. The left kidney was externalized for imaging as described previously[37]. Mice were positioned on a custom-built temperature-controlled stage with monitoring of body temperature during experiments. Imaging was conducted using a custom-built multiphoton microscope performing in an inverted configuration[38], and equipped by a broadband tunable laser (InSight DeepSee Dual Ultrafast Ti:Sapphire, Spectraphysics). Intravital imaging was achieved with an XLPlan N ×25/1.05 water immersion objective (Olympus) and emitted light was collected through four gallium-arsenide-phosphide photomultiplier tubes (Hamamatsu) in a non-descanned epifluorescence detection mode. GCaMP6s and Dextran Alexa 647 (2mg/kg) signals were imaged at 950nm and 1120nm, respectively. Signals were acquired every 1.35 seconds. After imaging, the area was marked with the laser to enable later recognition and kidney sections were fixed in 4% PFA for immunofluorescence staining.

Analysis of calcium signals

To analyze calcium activity in renal fibroblasts, recorded videos were firstly processed using FIJI image analysis software and regions of interest were manually drawn. An arbitrary threshold for detection of calcium transients was set as 2 x the lowest fluorescence intensity recorded. Thereafter, calcium activity was evaluated as percentage of fluorescence signal above the threshold.

Kidney disease models

Murine model of cisplatin-induced acute kidney injury

GCaMP6s mice were given *Cis*-diamminedichloroplatinum (II) (cisplatin, 20 mg/kg body weight) or vehicle (0.9% saline) by intraperitoneal injection, followed by imaging 72 hours after treatment[21].

Murine model of unilateral ureteric obstruction (UUO)

The left ureter was ligated to produce blockage of one kidney (hydronephrosis) using previously established proocols[39]. The procedure took place under general anesthesia (isoflurane) and analgesia (buprenorphine 0.1 mg/kg via s.c. injection). Mice were transferred to a warming chamber for recovery and kept there for 1 day post operatively. After 7 days animals underwent intravital imaging under general anaesthesia. To investigate the effect of P2Y6R inhibition, mice were injected with the antagonist MRS 2578 (3mg/kg, i.p.) five hours after the ureteric ligation, and once daily until day 7.

Murine model of folic acid nephropathy (FAN)

To induce chronic kidney disease, mice received a single injection of folic acid (250mg/kg, i.p.) as previously described[40]. To investigate the effect of P2Y6R inhibition, C57BL6 mice were injected with the antagonist MRS 2578 (3mg/kg, i.p.) five hours after folic acid injection, and once daily until day 14. A kinetic UV test for the quantitative determination of urea and an enzymatic assay for the quantitative determination of creatinine in mouse serum were performed using an AU480 Clinical Chemistry System, Beckman Coulter.

Histological and immunofluorescence staining of kidney sections

Frozen kidneys were sectioned at 5µm and 16µm. PFA-fixed, paraffin-embedded blocks were sectioned at 5µm, and antigen retrieval was performed at 110°C in citrate buffer at pH 6 for immunofluorescence staining. Thick cortical and medullary kidney sections after multiphoton imaging were fixed in 4% PFA.

Kidney sections were permeabilized with 0.1% TritonX-100 (Surfact-Amps detergent solution, Thermo Fisher Scientific) for 10 minutes for thin sections and 1 hour for thick sections. Next, tissue sections were blocked with 1% BSA and 10% donkey or goat serum before incubation overnight at 4°C with primary antibody.

The following primary antibodies were used for immunofluorescence staining: rabbit anti-PDGFRβ (Abcam, ab32570, 1:300 and 1:500), chicken anti-GFP (Aves, GFP-1020, 1:300 and 1:400), mouse anti-αSMA-Cy3 (Sigma, C6198, 1:300 and 1:500), rabbit anti-Fibronectin (Sigma, F3648, 1:200); mouse anti-Col1a1 (DSHB, F1C3, 1:100), rat anti-F4/80 (Biorad, MCA497GA, 1:50), rabbit anti-CDA (Thermo Fisher, PA5-76650, 1:100), mouse anti-Aquaporin 1 (Abcam, ab9566, 1:250). On the following day, sections were washed with PBS, and incubated at room temperature for 2 hours with the following secondary antibodies: donkey anti-rabbit-AF647 (711-606-152, Jackson ImmunoResearch Europe Ltd, 1:300 and 1:500), donkey anti-chicken-Cy3 (703-165-15, Jackson, 1:300 and 1:500), goat anti-mouse-AF568 (A-11004, Thermo Fisher Scientific, 1:500), goat anti-rat-Cy5 (112-607-003, Jackson ImmunoResearch Europe Ltd, 1:500). After incubation with secondary antibodies, sections were washed with PBS, and cellular DNA was stained with 10µg/ml Hoechst 33342 (H1399, Molecular Probes) for 5 minutes at room temperature. Slices were mounted with Dako mounting medium (Agilent, Santa Clara). Visualization of the staining was performed with an Axio Scan.Z1 slidescanner using a Plan Apochromat 40x/0.95 air immersion objective, a confocal Leica SP8 inverse STED 3X microscope using an HC PL APO CS2 20x/0.75 oil immersion objective, and an inverted confocal laser scanning microscope ZEISS LSM 980 Airyscan by using a LD LCI Plan-Apochromat 25x/0.8 silicon-oil objective.

Collagen fibers were detected by staining the kidney sections according to sirius red/fast green protocol[41]. After deparaffinization, sections were washed with PBS and thereafter with distilled water for 5 minutes. Next, tissue was incubated in 0.04% fast green solution for 15 minutes and washed with distilled water. After incubating in 0.1% fast green/0.04% Sirius red in saturated picric acid solution for 30 minutes,

sections were washed with acidified water (0.5% acetic acid in distilled water). Subsequently, sections were dehydrated in 70%, 80%, 96%, and 100% ethanol, cleared with three changes of Histoclear and mounted. Visualization of the collagen staining was performed with an Axio Scan.Z1 slidescanner using a Plan Apochromat 20x/0.8 air immersion objective.

Image analysis

All images for comparison were taken using the same settings. Image processing was done in FIJI[42] and Zeiss ZEN. Regions of interest were drawn manually to obtain fluorescent signals. Brightness and contrast were optimized and applied to all parts of the figures equally for better visualization of the images. Nuclei counting in fibroblast proliferation experiments was performed in CellProfiler[43]. Figures were created with BioRender.com.

snRNA Sequencing Analysis

Data sets from the IRI models (GSE151167, GSE139107) and the POD-ATTAC model (GSE218376) were analyzed for *P2ry6* and *Cda* gene expression. Visualization of gene expression was performed using the VlnPlot and FeaturePlot functions in Seurat. Inferred RNA expression was calculated using Magic RNA, while gene set enrichment scores were computed with the AddModuleScore function in Seurat. The analysis was conducted using R version 4.3.1 and Seurat object version 4.

Statistical analysis

Data are presented as mean values (± SEM). All data were analyzed and displayed using GraphPad Prism software (GraphPad Prism version 10.0.0 for Windows, GraphPad Software, Boston, Massachusetts USA, www.graphpad.com). The following normality and lognormality tests were used: D'Agostino & Pearson test, Anderson-Darling test, Shapiro-Wilk test, and Kolmogorov-Smirnov test. Based on normal or non-normal data distribution, a suitable test was used to compare two groups. *P* values of less than 0.05 were considered statistically significant.

Data availability

All data relevant to judge and interpret this study were included in the paper and its accompanying Supplementary Information and Source Data Files. The snRNA-seq datasets used in this study were previously published and are publicly available in the Gene Expression Omnibus under accession codes GSE151167, GSE139107, and GSE218376: www.ncbi.nlm.nih.gov/geo/query/acc.cgi?acc=GSE151167, www.ncbi.nlm.nih.gov/geo/query/acc.cgi?acc=GSE139107, www.ncbi.nlm.nih.gov/geo/query/acc.cgi?acc=GSE218376

References

1. Kalantar-Zadeh, K., Jafar, T. H., Nitsch, D., Neuen, B. L. & Perkovic, V. Chronic kidney disease. *Lancet* **398**, 786–802 (2021).

2. Luyckx, V. A. *et al.* Mind the gap in kidney care: translating what we know into what we do. *Kidney Int* **105**, 406–417 (2024).

3. Francis, A. *et al.* Chronic kidney disease and the global public health agenda: an international consensus. *Nature Reviews Nephrology 2024 20:7* **20**, 473–485 (2024).

4. Chrysopoulou, M. & Rinschen, M. M. Metabolic Rewiring and Communication: An Integrative View of Kidney Proximal Tubule Function. *Annual Review of Physiology Downloaded from www.annualreviews.org. Guest* **11**, 21 (2025).

5. Quinn, G. Z., Dhillon, P. & Susztak, K. It Takes Two to Tango: The Role of Dysregulated Metabolism and Inflammation in Kidney Disease Development. *Semin Nephrol* **40**, 199–205 (2020).

6. Lee, L. E., Doke, T., Mukhi, D. & Susztak, K. The key role of altered tubule cell lipid metabolism in kidney disease development. *Kidney Int* https://doi.org/10.1016/J.KINT.2024.02.025 (2024) doi:10.1016/J.KINT.2024.02.025.

7. Miguel, V., Shaw, I. W. & Kramann, R. Metabolism at the crossroads of inflammation and fibrosis in chronic kidney disease. *Nature Reviews Nephrology 2024* 1–18 (2024) doi:10.1038/s41581-024-00889-z.

8. Kaissling, B. & Le Hir, M. The renal cortical interstitium: Morphological and functional aspects. *Histochem Cell Biol* **130**, 247–262 (2008).

9. Humphreys, B. D. Mechanisms of Renal Fibrosis. *Annual Review of Physiology* vol. 80 309–326 Preprint at https://doi.org/10.1146/annurev-physiol-022516-034227 (2018).

10. Sato, Y., Takahashi, M. & Yanagita, M. Pathophysiology of AKI to CKD progression. *Semin Nephrol* **40**, 206–215 (2020).

11. Li, L., Fu, H. & Liu, Y. The fibrogenic niche in kidney fibrosis: components and mechanisms. *Nature Reviews Nephrology 2022 18:9* **18**, 545–557 (2022).

12. Tanaka, S., Portilla, D. & Okusa, M. D. Role of perivascular cells in kidney homeostasis, inflammation, repair and fibrosis. *Nature Reviews Nephrology 2023 19:11* **19**, 721–732 (2023).

13. Lane, A. N. & Fan, T. W. M. Regulation of mammalian nucleotide metabolism and biosynthesis. *Nucleic Acids Res* **43**, 2466–2485 (2015).

14. Kirita, Y., Wu, H., Uchimura, K., Wilson, P. C. & Humphreys, B. D. Cell profiling of mouse acute kidney injury reveals conserved cellular responses to injury. *Proc Natl Acad Sci U S A* **117**, 15874–15883 (2020).

15. Legouis, D. *et al.* Altered proximal tubular cell glucose metabolism during acute kidney injury is associated with mortality. *Nature Metabolism 2020 2:8* **2**, 732–743 (2020).

16. Rinaldi, A. *et al.* Impaired fatty acid metabolism perpetuates lipotoxicity along the transition to chronic kidney injury. *JCI Insight* **7**, (2022).

17. Scolaro, T. *et al.* Nucleotide metabolism in cancer cells fuels a UDP-driven macrophage cross-talk, promoting immunosuppression and immunotherapy resistance. *Nature Cancer 2024 5:8* **5**, 1206–1226 (2024).

18. Faivre, A. *et al.* Spatiotemporal Landscape of Kidney Tubular Responses to Glomerular Proteinuria. *Journal of the American Society of Nephrology* https://doi.org/10.1681/ASN.0000000000000357 (2024) doi:10.1681/ASN.0000000000000357.

19. Bar, I. *et al.* Knockout Mice Reveal a Role for P2Y6 Receptor in Macrophages, Endothelial Cells, and Vascular Smooth Muscle Cells. *Mol Pharmacol* **74**, 777–784 (2008).

20. Ito, M. & Matsuoka, I. Inhibition of P2Y6 receptor-mediated phospholipase C activation and Ca2+ signalling by prostaglandin E2 in J774 murine macrophages. *Eur J Pharmacol* **749**, 124–132 (2015).

21. Martins, J., Haenni, D., Bugarski, M., Figurek, A. & Hall, A. M. Quantitative intravital calcium imaging maps single cell behavior to kidney tubular structure. *American Journal of Physiology-Renal Physiology* ajprenal.00052.2020 (2020) doi:10.1152/ajprenal.00052.2020.

22. Lazarowski, E. R. & Boucher, R. C. UTP as an extracellular signaling molecule. *News Physiol Sci* **16**, 1–5 (2001).

23. Persaud, A. K. *et al.* Increased renal elimination of endogenous and synthetic pyrimidine nucleosides in concentrative nucleoside transporter 1 deficient mice. *Nature Communications 2023 14:1* **14**, 1–19 (2023).

24. Schiessl, I. M. *et al.* Renal interstitial platelet-derived growth factor receptor-β cells support proximal tubular regeneration. *Journal of the American Society of Nephrology* **29**, 1383–1396 (2018).

25. Saliba, Y. *et al.* Evidence of a role for fibroblast transient receptor potential canonical 3 Ca2+ channel in renal fibrosis. *Journal of the American Society of Nephrology* **26**, 1855–1876 (2015).

26. Nishida, M. *et al.* P2Y6 receptor-Gα12/13 signalling in cardiomyocytes triggers pressure overload-induced cardiac fibrosis. *EMBO Journal* **27**, 3104–3115 (2008).

27. Umpierre, A. D. *et al.* Microglial P2Y6 calcium signaling promotes phagocytosis and shapes neuroimmune responses in epileptogenesis. *Neuron* **112**, 1959-1977.e10 (2024).

28. Daghbouche-Rubio, N. *et al.* The P2Y6 Receptor as a Potential Keystone in Essential Hypertension. *Function* **5**, 1–15 (2024).

29. Zhang, S. *et al.* Sensing ceramides by CYSLTR2 and P2RY6 to aggravate atherosclerosis. *Nature* **641**, 476–485 (2025).

30. Kuppe, C. *et al.* Decoding myofibroblast origins in human kidney fibrosis. *Nature 2020 589:7841* **589**, 281–286 (2020).

31. Sohn, S. J. *et al.* In vitro evaluation of biomarkers for cisplatin-induced nephrotoxicity using HK-2 human kidney epithelial cells. *Toxicol Lett* **217**, 235–242 (2013).

32. Liang, C. C., Park, A. Y. & Guan, J. L. In vitro scratch assay: a convenient and inexpensive method for analysis of cell migration in vitro. *Nature Protocols 2007 2:2* **2**, 329–333 (2007).

33. Livak, K. J. & Schmittgen, T. D. Analysis of Relative Gene Expression Data Using Real-Time Quantitative PCR and the 2−ΔΔCT Method. *Methods* **25**, 402–408 (2001).

34. Madisen, L. *et al.* Transgenic mice for intersectional targeting of neural sensors and effectors with high specificity and performance. *Neuron* **85**, 942–58 (2015).

35. Schwenk, F., Baron, U. & Rajewsky, K. A cre-transgenic mouse strain for the ubiquitous deletion of loxP-flanked gene segments including deletion in germ cells. *Nucleic Acids Res* **23**, 5080–5081 (1995).

36. Müller, T. *et al.* P2Y6 receptor activation promotes inflammation and tissue remodeling in pulmonary fibrosis. *Front Immunol* **8**, 282412 (2017).

37. Schuh, C. D. *et al.* Long wavelength multiphoton excitation is advantageous for intravital kidney imaging. *Kidney Int* **89**, 712–9 (2016).

38. Mayrhofer, J. M. *et al.* Design and performance of an ultra-flexible two-photon microscope for in vivo research. *Biomed Opt Express* **6**, 4228 (2015).

39. Chevalier, R. L., Forbes, M. S. & Thornhill, B. A. Ureteral obstruction as a model of renal interstitial fibrosis and obstructive nephropathy. *Kidney Int* **75**, 1145–1152 (2009).

40. Yang, H. C., Zuo, Y. & Fogo, A. B. Models of chronic kidney disease. *Drug Discov Today Dis Models* **7**, 13–19 (2010).

41. Segnani, C. *et al.* Histochemical Detection of Collagen Fibers by Sirius Red/Fast Green Is More Sensitive than van Gieson or Sirius Red Alone in Normal and Inflamed Rat Colon. *PLoS One* **10**, e0144630–e0144630 (2015).

42. Schindelin, J. *et al.* Fiji: An open-source platform for biological-image analysis. *Nature Methods* vol. 9 676–682 Preprint at https://doi.org/10.1038/nmeth.2019 (2012).

43. Stirling, D. R. *et al.* CellProfiler 4: improvements in speed, utility and usability. *BMC Bioinformatics* **22**, 1–11 (2021).

Acknowledgements

The authors acknowledge support from The Center for Microscopy and Image Analysis, University of Zurich. This work was supported by The Swiss National Centre for Competence in Research (NCCR) Kidney Control of Homeostasis (Grant ID: 183774) and a Swiss National Science Foundation project grant (310030_184688). Work in the P.E.C laboratory is supported by the Balli and Gianella foundations and Ente Ospedaliero Cantonale Junior Grant.

Author contributions

Conceptualization: A.M.H. Experimentation: A.F., N.J., S.K., M.K., I.S., and B.R. Data analysis: A.F., N.J., A.R. P.C., and B.R. Funding acquisition: A.M.H. Project supervision: A.M.H. Writing—original draft: A.F. and A.M.H. Writing—review and editing: all authors.

Competing interests

The authors declare no competing interests.

Figure legends

Fig. 1. Pyrimidine metabolism in the mouse kidney. (a) Uniform manifold approximation and projection (UMAP) plot of kidney samples analysed by snRNAseq and integrated (n=32; 60’360 renal nuclei) identifies the different cellular components of the kidney. Featureplot (lower panel) showing enrichment score of pyrimidine metabolism genes calculated using addmodule score on Magic Assay RNA (custom list of genes included cda, enpp1, enpp3, nudt2, dhodh, cad, umps, dctpp1). Proximal Tubule Segment S1, S2, S3; new (injured) proximal tubule clusters (PT0, PT1, PT2, PT3, PT4); DTL, descending limb of loop of Henle; ATL,

thin ascending limb of loop of Henle; TAL, thick ascending limb of loop of Henle (TAL1, TAL2, TAL3); POD, podocytes; Distal nephron (cluster DN1, DN2, DN3, DN4); ICA, type A intercalated cells of collecting duct; ICB, type B intercalated cells of collecting duct; PC, principle cells; EC, endothelial cells, Immune and Stroma cells. (b) Vlnplot showing Cda gene expression across cell type and cell states during disease progression in an ischemia-reperfusion model (acute phase = 4-96 hours, chronic phase = 2-6 weeks). The Control group served as the reference (n= 6 sham and n=3 normal kidneys). Magic Assay RNA Violin plots show the distribution of expression of Cda; overlaid box plots display the median (centre line), 25th and 75th percentiles (box), and minima/maxima within 1.5×IQR (whiskers). Individual points are not shown, n corresponds to the number of independent single cells analyzed per group: n = 27,569 nuclei from n=9 mice for Control, n = 18,886 nuclei from n=14 mice for Early, and n = 13,905 nuclei from n=9 mice for Late. Each cell is a biological replicate; no technical replicates were included in the statistical comparisons. (c) Antibody staining showing increased CDA abundance in aquaporin 1 (AQP1) positive proximal tubular cells in unilateral ureteric obstruction (UUO) and folic acid nephropathy (FAN) disease models, with surrounding fibroblasts positive for αSMA. Scale bars 30 µm. (d) Quantitative RT-PCR indicates an upregulation of the CDA gene, along with injury markers HAVCR1 (KIM-1) and LCN2 (NGAL), in cisplatin- and folic acid- induced injury models in human kidney proximal tubular cells (HK-2) (biological triplicates; technical triplicates depicted as single dots; mean ± SEM, two-sided unpaired t-test, **p=0.0011,***p=0.0002, ****p<0.0001). (e) Extracellular UDP measurements in injured HK-2 cells (biological triplicates; mean ± SEM, two-sided unpaired t-test, *p=0.0500, **p=0.0065).

Fig. 2. P2Y6 receptor expression and activation in kidney fibroblasts. (a-b) Expression of the P2ry6 gene was increased in stromal (interstitial) cells in single cell sequencing studies of kidneys from C57BL/6J mice exposed to ischemia-reperfusion injury (IRI: early = 4-96 hours, late = 2-6 weeks) or in a transgenic mouse model of inducible glomerular proteinuria (POD-ATTAC). Pairwise comparisons using Wilcoxon rank sum test with continuity correction. P value adjustment method: fdr, *ad-p value <0.05. Box plots show the

median (center line), 25th and 75th percentiles (box), and minima/maxima within 1.5×IQR (whiskers). Individual points represent expression values of P2ry6 for each single cell. Each data point shown is one independent cell; no technical replicates were used for statistical testing. Cells were assigned to three groups based on sample phase: Control, Early, and Late. The Control group served as the reference. Final sample sizes plotted are: n = 1,084 nuclei from n=9 mice for Control, n =161 nuclei from n=14 mice for Early, and n = 300 nuclei from n=9 mice for Late, exactly matching the number of data points shown for the IRI dataset. Final sample sizes plotted are: n = 1,459 nuclei from n=3 mice for Control, n =1,152 nuclei from n=3 mice for 7d, and n = 2,165 nuclei from n=4 mice for 28d, exactly matching the number of data points shown for the POD dataset. Magic RNA is shown. (c-d) P2Y6R mRNA expression in whole kidneys measured by RT-qPCR is increased in UUO (n=5) and folic acid nephropathy (n=10/4) in wildtype (WT) mice. P2Y6 knockout (KO) mice were used as a control. LK = left kidney, RK = right kidney. Data are presented as mean ± SEM, two-sided unpaired t-test, **p=0.0012, ****p<0.0001. (e) P2Y6 receptor activation by UDP (50 µM) or a P2Y6 agonist (MRS2957, 10 µM) induced acute rises in intracellular calcium in interstitial fibroblasts (red arrows) in kidney slices prepared from GCaMP6s expressing mice, which were inhibited by the non-specific purinergic blocker suramin (50 µM) or a specific P2Y6 antagonist (MRS2578, 10 µM). The experiment was independently repeated in three mice with similar results. Scale bars 10 µm. (f) Example traces for each experiment. (g) Quantification of signals (n=3 biological replicates (mice), mean ± SEM, Friedman test, ***p=0.0003, ****p<0.0001). For each mouse, at least one video was acquired and analyzed. Multiple ROIs were quantified per video; ROIs represent technical measurements (fibroblasts) and are shown as individual points. Image sequences displaying propagation of calcium signals from cell processes towards the cell body after application of UDP (50 µM) (h) or a P2Y6 agonist (10 µM) (j) in NRK-49F cells transfected with GCaMP6s. Scale bars 10 µm. (i and k) Quantification of fluorescent signals (n=5 independent experiments, mean ± SEM, Wilcoxon test, ****p<0.0001). Points represent individual fibroblast cells (ROIs); ROIs are technical measurements.

Fig. 3. Functional effects of P2Y6 receptor activation in kidney fibroblasts. (a) UDP (50 µM) and a P2Y6 agonist (MRS2957, 5 µM) induced proliferation of NRK-49F cells after 24h (n=4 independent biological experiments. For each experiment, three wells were plated and imaged. Twenty-five fields of view were acquired per well. Individual points represent single nuclei and constitute technical measurements, mean ± SEM, Kruskal-Wallis test, *p=0.0480, **p=0.0014). (b) P2Y6 agonist (5 µM) promotes migration of NRK-49F cells after 24h (n=3 independent biological experiments. For each experiment, three images were acquired, and four distance measurements were taken per image. Individual points represent single distance measurements (technical measurements), mean ± SEM, two-sided unpaired t-test, ****p<0.0001). (c) Pre-treatment with a calcium chelator (20 µM BAPTA) for 30min prevents proliferation (n=4 independent biological experiments. For each experiment, three wells were plated and imaged. Twenty-five fields of view were acquired per well. Individual points represent single nuclei and constitute technical measurements, mean ± SEM, Kruskal-Wallis test, ***p=0.0004, ****p<0.0001). (d) Treatment with a specific P2Y6 antagonist (MRS2578, 1 µM) prevents P2Y6 agonist-induced proliferation (n=3 independent biological experiments. For each experiment, three wells were plated and imaged. Twenty-five fields of view were acquired per well. Individual points represent single nuclei and constitute technical measurements, mean ± SEM, Kruskal-Wallis test, *p=0.0346, ***p=0.0004). (e) Quantitative RT-PCR reveals up-regulation of genes involved in fibroblast proliferation (MIK67), myofibroblast activation (PDGFRβ, αSMA, Fibronectin, Vimentin) and collagen I production in NRK-49F cells treated with a P2Y6 agonist (10 µM) over 24h (biological triplicates; technical quadruplicates depicted as single dots; mean ± SEM, two-sided t-test; **p=0.0068 (Vimentin), **p=0.0030 (Collagen I), ***p=0.0003 (αSMA), ***p=0.0002 (Fibronectin), ****p<0.0001). (f-g) Antibody staining showing that P2Y6 agonist (10 µM) treatment after 72h increases expression of pro-fibrotic markers fibronectin (f) and vimentin (g). Quantification of signals (n=3 independent biological experiments, five technical replicates, individual

points represent single fibroblasts identified within the images (technical measurements), mean ± SEM, Mann-Whitney test, ****p<0.0001). Scale bars 30 µm. AG = agonist; ANT = antagonist.

Fig. 4. Kidney fibroblasts display spontaneous calcium signals arising in processes. (a) Fixation of cortical kidney tissue after intravital imaging in GCaMP6s expressing mice (created in BioRender. Figurek, A. (2025) https://BioRender.com/ o23b795) and (b) immunostaining with anti-PDGFRβ antibody enables identification of renal fibroblasts (scale bar 50 µm). (c) Sum image of 405s showing calcium activity in kidney cortex ("#" marks proximal tubular cell and "*" fibroblast, scale bar 50 µm). Experiment was independently repeated in three mice with similar results (b-c). (d-e) Fibroblasts display an irregular pattern of spontaneous calcium activity compared to discrete transients in neighboring proximal tubular cells. (f) Slices of mouse kidney were used to image intracellular calcium propagation in fibroblasts in more detail. Created in BioRender. Figurek, A. (2025) https://BioRender.com/ b45m156. (g) Retrospective antibody staining identified PDGFRβ positive fibroblasts (scale bar 10 µm). (h) Corresponding sum image of GCaMP6s signal (43s, "*" marks fibroblast, scale bar 10 µm). Experiment was independently repeated in three mice with similar results (g-h). (i) Irregular calcium transients in fibroblasts in freshly cut kidney slices. (j) Example of calcium signal propagation (arrow) from a fibroblast process across the cell body. Images were acquired every 0.43s. Scale bar 10 nm.

Fig. 5. Calcium activity in kidney fibroblasts increases in disease models. (a) Acute tubular injury was induced by injecting GCaMP6s mice with 20 mg/kg cisplatin i.p. Created in BioRender. Figurek, A. (2025) https://BioRender.com/ o07l816. (b) Sum image (405s) and color-coded images of calcium transients in vehicle treated mice. Color denotes when signal appears during the recording period. (c) Calcium activity was decreased in proximal tubules (PTs) damaged by cisplatin but increased in surrounding fibroblasts (arrows). (d-e) Quantification of calcium activity in fibroblasts and tubules (n=5 biological replicates (mice), one intravital video was acquired per mouse. Individual points represent fibroblasts (d) or proximal tubules (e) identified within each video and constitute technical measurements; mean ± SEM, Mann-

Whitney test, ****p<0.0001). Scale bars 50 µm. (f) Sum (135s, left panels) and temporal color-coded images of calcium activity in sham mice. Uptake of filtered dextran indicates normal tubular function. (g) In unilateral ureteric obstruction (UUO) mice the filtration and uptake of dextran was severely impaired. Calcium activity was decreased in PTs, but substantially increased in fibroblasts (arrows). (h-i) Quantification of calcium activity in fibroblasts and tubules (n=4 biological replicates (mice), one intravital video was acquired per mouse. Individual points represent fibroblasts (h) or proximal tubules (i) identified within each video and constitute technical measurements; mean ± SEM, Mann-Whitney, ***p<0.001, ****p<0.0001). Scale bars 50 µm. (j-k) Antibody staining for fibroblasts (PDGFRβ) and myofibroblasts (αSMA) showing massive proliferation in UUO compared to sham. Scale bars 30 µm. (l-m) Quantification of signals (n=4 biological replicates (mice), three images per mouse were acquired. Individual points represent number of fibroblasts (l) or myofibroblasts (m) identified within each image and constitute technical measurements; mean ± SEM, two-sided unpaired t-test and Mann-Whitney test, ****p<0.0001).

Fig. 6. P2Y6 receptor knock-out decreases proliferation of renal fibroblasts and fibrosis in a ureteric obstruction model. (a) Schematic representation of the experimental protocol. Created in BioRender. Figurek, A. (2025) https://BioRender.com/o26n540. (b) Antibody staining showing significant decrease in fibroblast proliferation (PDGFRβ), myofibroblast activation (fibronectin, αSMA), macrophage infiltration (F4/80), and collagen 1 production (Col1) in P2Y6 KO mice at 7 days following UUO. Scale bars 50 µm. P2Y6 KO mice have less kidney fibrosis stained by sirius red compared to wild-type (WT) mice. Scale bars 100 µm. (c) Quantification of signals (n=10 WT mice/9 KO mice, three images per mouse were acquired. Individual points represent cell number or area stained identified within each image; mean ± SEM, two-sided unpaired t-test and Mann-Whitney test, **p=0.0041 (fibronectin), **p=0.0087 (αSMA), **p=0.0021 (F4/80), ***p=0.0007 (PDGFRβ), ***p=0.0001 (collagen 1), ****p<0.0001).

Fig. 7. Inhibition of the P2Y6 receptor decreases proliferation of renal fibroblasts and fibrosis in a ureteric obstruction model. (a) Schematic representation of the experimental protocol. Created in

BioRender. Figurek, A. (2025) https://BioRender.com/ftjh94s. (b) Antibody staining showing a significant decrease in fibroblast proliferation (PDGFRβ), myofibroblast activation (fibronectin, αSMA), macrophage infiltration (F4/80), and collagen 1 production (Col1) in mice treated daily with a P2Y6 antagonist (MRS2578, 3mg/kg) i.p. at 7 days following UUO. Scale bars 50 µm. P2Y6 antagonist-treated mice had less kidney fibrosis stained by sirius red compared to control mice following UUO. Scale bars 100 µm. (c) Quantification of signals (n=7 mice treated with a P2Y6 antagonist /5 control mice, three images per mouse were acquired. Individual points represent cell number or area stained identified within each image; mean ± SEM, two-sided unpaired t-test and Mann-Whitney test, *p=0.0178, **p=0.0053, ***p=0.0001, ****p<0.0001).

Fig. 8. P2Y6 receptor knock-out decreases proliferation of renal fibroblasts, fibrosis, and improves kidney function in a folic acid model of CKD. (a) Schematic representation of the experimental model. Created in BioRender. Figurek, A. (2025) https://BioRender.com/y48u718. (b) Antibody staining showing significant decrease in fibroblast proliferation (PDGFRβ), myofibroblast activation (fibronectin, αSMA), macrophage infiltration (F4/80), and collagen 1 production (Col1) in P2Y6 KO mice with folic acid nephropathy (FAN). Scale bars 50 µm. P2Y6 KO mice have less kidney fibrosis stained by sirius red compared to P2Y6 wild-type (WT) mice with FAN. Scale bars 100 µm. (c) Quantification of signals (n=8 KO mice/9 WT mice, three images per mouse were acquired. Individual points represent cell number or area stained identified within each image; mean ± SEM, two-sided unpaired t-test and Mann-Whitney test, *p=0.0142, ***p=0.0001, ****p<0.0001). (D) P2Y6 KO mice had significantly lower serum urea and creatinine values compared to WT mice with FAN (n=8 KO mice /9 WT mice, two-sided unpaired t-test, **p=0.0025 (urea), **p=0.0095 (creatinine)).

Fig. 9. Inhibition of the P2Y6 receptor decreases proliferation of renal fibroblasts and fibrosis in a folic acid model of CKD. (a) Schematic representation of the experimental model. Created in BioRender. Figurek, A. (2025) https://BioRender.com/r30i414. (b) Antibody staining showing significant decrease in

fibroblast proliferation (PDGFRβ), myofibroblast activation (fibronectin, αSMA), macrophage infiltration (F4/80), and collagen 1 production (Col1) in mice with folic acid nephropathy (FAN) treated with a P2Y6 antagonist (MRS2578) compared to vehicle. Scale bars 50 μm. P2Y6 antagonist-treated mice had less kidney fibrosis stained by sirius red compared to vehicle treated. Scale bars 100 μm. (c) Quantification of signals (n=6 mice in each group, three images per mouse were acquired. Individual points represent cell number or area stained identified within each image; mean ± SEM, two-sided unpaired t-test and Mann-Whitney test,**p=0.0011 (αSMA), ,**p=0.0045 (collagen 1), ,**p=0.0018 (sirius red),***p=0.0003 (fibronectin), ****p<0.0001). (D) Mice treated with a P2Y6 antagonist had lower serum urea and creatinine values compared to control mice with FAN (n=6 mice in each group, two-sided unpaired t-test, p=0.6390 (urea), p=0.5529 (creatinine)).

Fig. 10. Proposed mechanism of tubulo-interstitial crosstalk in chronic kidney disease. Injury to tubular cells causes extracellular release of UDP, which can activate P2Y6 receptors on neighboring fibroblasts (1), resulting in intracellular calcium release (2-3). This then stimulates gene expression changes (4), leading to fibroblast proliferation, migration, and conversion to a myofibroblast phenotype (5), ultimately driving collagen deposition and organ fibrosis. Image created in BioRender. Figurek, A. (2025) https://BioRender.com/ s29s214.

Editor's Summary

Fibrosis is the final common pathway in chronic kidney disease and a potential target for therapeutic interventions. Here, the authors use intravital imaging to show that pyrimidinergic calcium signaling links tubular injury to fibroblast activation, and that blocking this pathway reduces fibrosis

Peer review information: *Nature Communications* thanks Matthias Hackl, and the other, anonymous, reviewer(s) for their contribution to the peer review of this work. A peer review file is available.

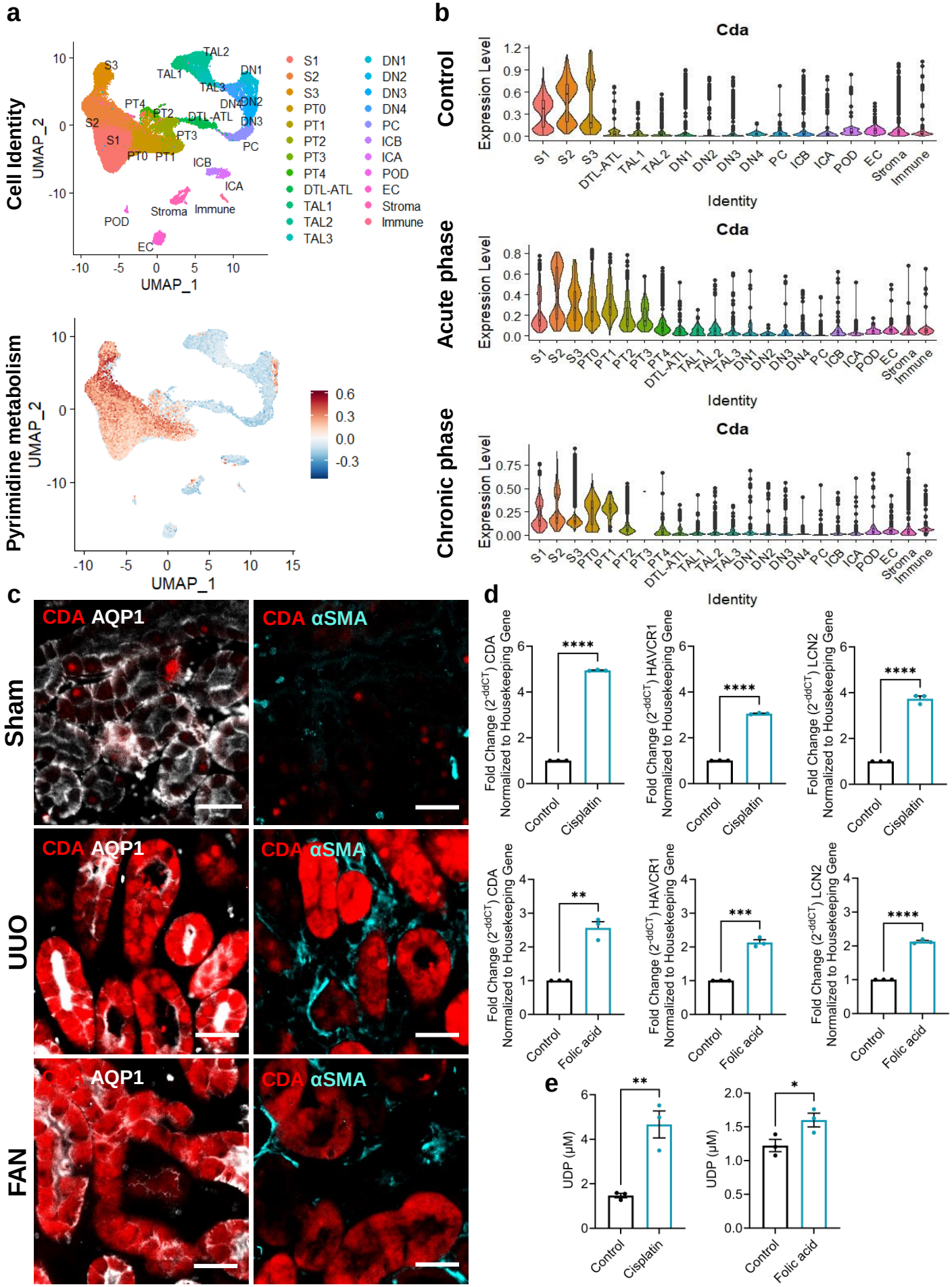
a
Cell Identity
UMAP_2
UMAP_1
S1
S2
S3
PT0
PT1
PT2
PT3
PT4
DTL-ATL
TAL1
TAL2
TAL3
DN1
DN2
DN3
DN4
PC
ICB
ICA
POD
EC
Stroma
Immune
Pyrimidine metabolism
b
Control
Acute phase
Chronic phase
Cda
Expression Level
Identity
c
Sham
UUO
FAN
CDA AQP1
CDA αSMA
d
Fold Change (2-ddCT) CDA Normalized to Housekeeping Gene
Fold Change (2-ddCT) HAVCR1 Normalized to Housekeeping Gene
Fold Change (2-ddCT) LCN2 Normalized to Housekeeping Gene
Control
Cisplatin
Folic acid
e
UDP (μM)

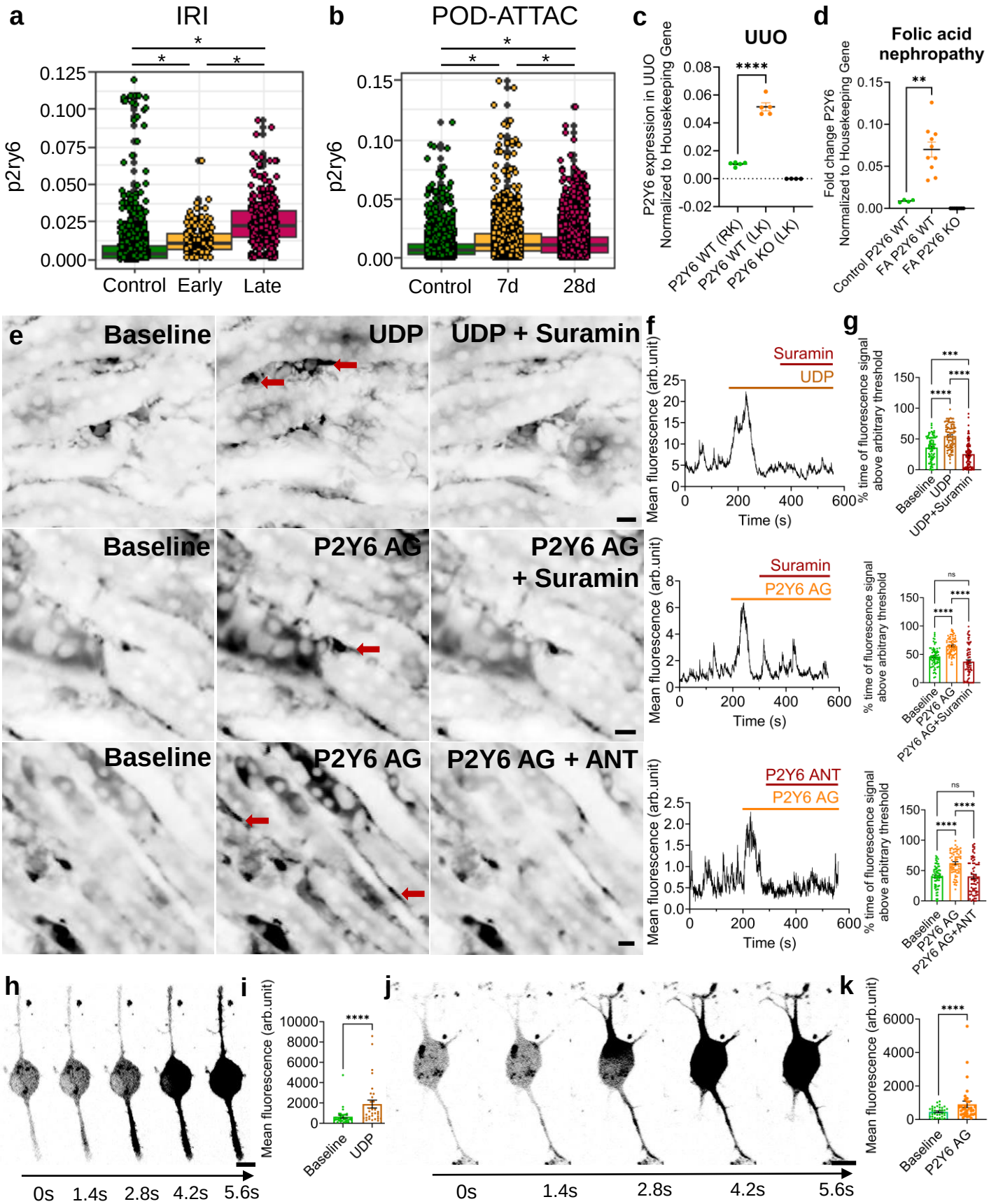
a
IRI
p2ry6
Control
Early
Late
b
POD-ATTAC
p2ry6
Control
7d
28d
c
UUO
P2Y6 expression in UUO Normalized to Housekeeping Gene
****
P2Y6 WT (RK)
P2Y6 WT (LK)
P2Y6 KO (LK)
d
Folic acid nephropathy
Fold change P2Y6 Normalized to Housekeeping Gene
**
Control P2Y6 WT
FA P2Y6 WT
FA P2Y6 KO
e
Baseline
UDP
UDP + Suramin
Baseline
P2Y6 AG
P2Y6 AG + Suramin
Baseline
P2Y6 AG
P2Y6 AG + ANT
f
Suramin
UDP
Mean fluorescence (arb.unit)
Time (s)
Suramin
P2Y6 AG
Mean fluorescence (arb.unit)
Time (s)
P2Y6 ANT
P2Y6 AG
Mean fluorescence (arb.unit)
Time (s)
g
% time of fluorescence signal above arbitrary threshold
Baseline
UDP
UDP+Suramin
% time of fluorescence signal above arbitrary threshold
Baseline
P2Y6 AG
P2Y6 AG+Suramin
% time of fluorescence signal above arbitrary threshold
Baseline
P2Y6 AG
P2Y6 AG+ANT
h
0s
1.4s
2.8s
4.2s
5.6s
i
Mean fluorescence (arb.unit)
****
Baseline
UDP
j
0s
1.4s
2.8s
4.2s
5.6s
k
Mean fluorescence (arb.unit)
****
Baseline
P2Y6 AG

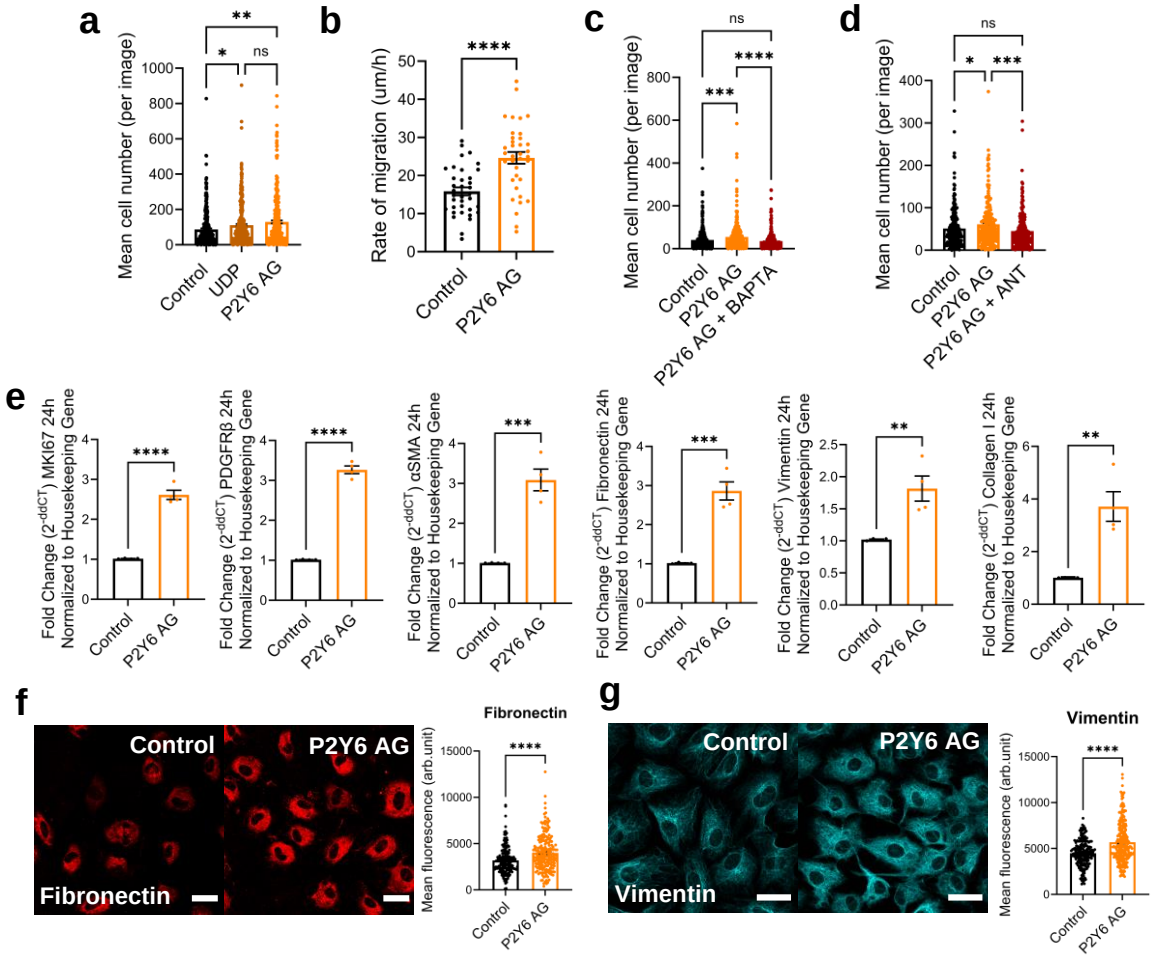
a
Mean cell number (per image)
Control
UDP
P2Y6 AG
b
Rate of migration (um/h)
Control
P2Y6 AG
c
Mean cell number (per image)
Control
P2Y6 AG
P2Y6 AG + BAPTA
d
Mean cell number (per image)
Control
P2Y6 AG
P2Y6 AG + ANT
e
Fold Change (2-ddCT) MKI67 24h Normalized to Housekeeping Gene
Fold Change (2-ddCT) PDGFRβ 24h Normalized to Housekeeping Gene
Fold Change (2-ddCT) αSMA 24h Normalized to Housekeeping Gene
Fold Change (2-ddCT) Fibronectin 24h Normalized to Housekeeping Gene
Fold Change (2-ddCT) Vimentin 24h Normalized to Housekeeping Gene
Fold Change (2-ddCT) Collagen I 24h Normalized to Housekeeping Gene
Control
P2Y6 AG
f
Control
P2Y6 AG
Fibronectin
Fibronectin
Mean fluorescence (arb.unit)
g
Control
P2Y6 AG
Vimentin
Vimentin
Mean fluorescence (arb.unit)

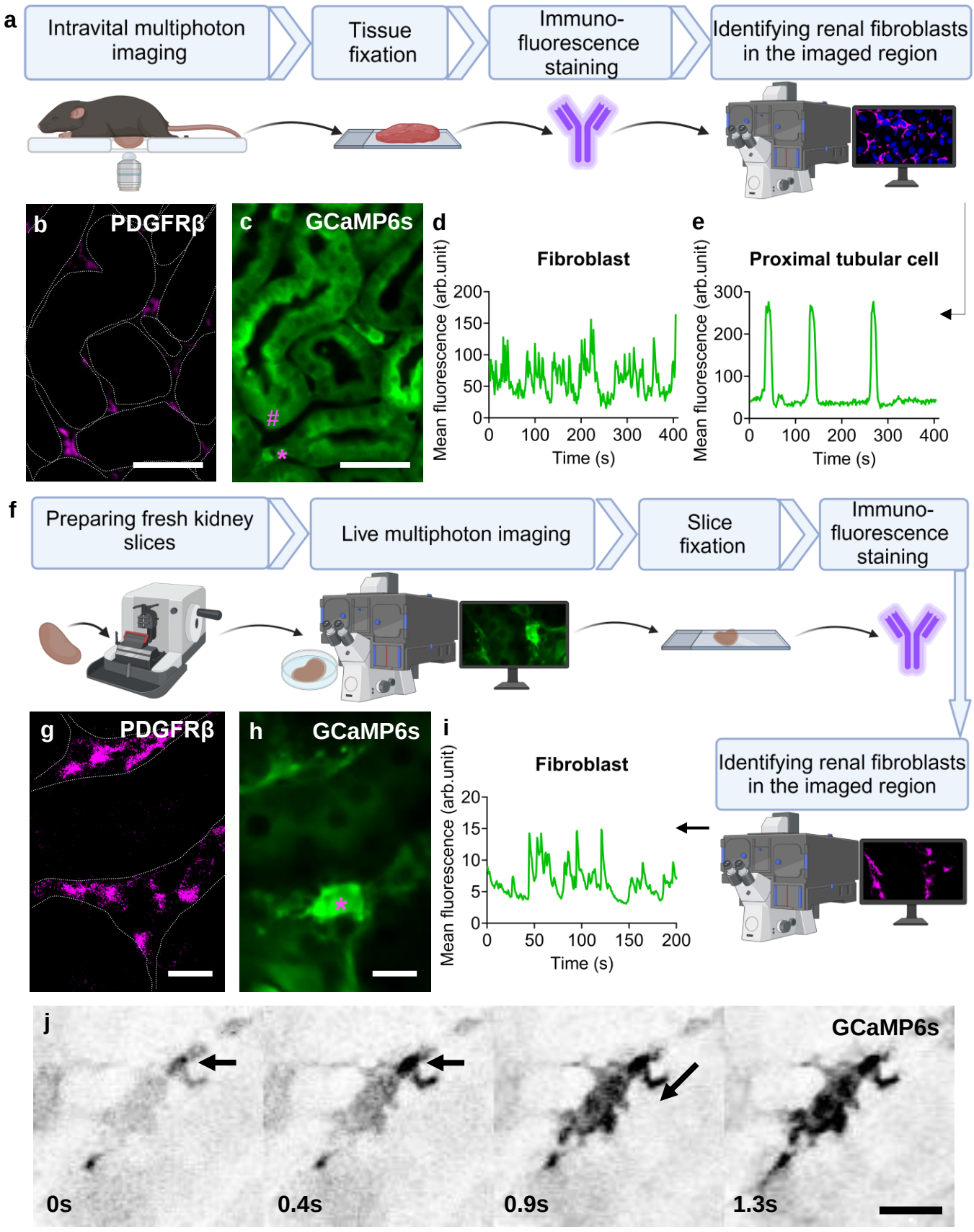
a
Intravital multiphoton imaging
Tissue fixation
Immuno-fluorescence staining
Identifying renal fibroblasts in the imaged region
b
PDGFRβ
c
GCaMP6s
#
*
d
Fibroblast
Mean fluorescence (arb.unit)
Time (s)
e
Proximal tubular cell
Mean fluorescence (arb.unit)
Time (s)
f
Preparing fresh kidney slices
Live multiphoton imaging
Slice fixation
Immuno-fluorescence staining
Identifying renal fibroblasts in the imaged region
g
PDGFRβ
h
GCaMP6s
*
i
Fibroblast
Mean fluorescence (arb.unit)
Time (s)
j
GCaMP6s
0s
0.4s
0.9s
1.3s

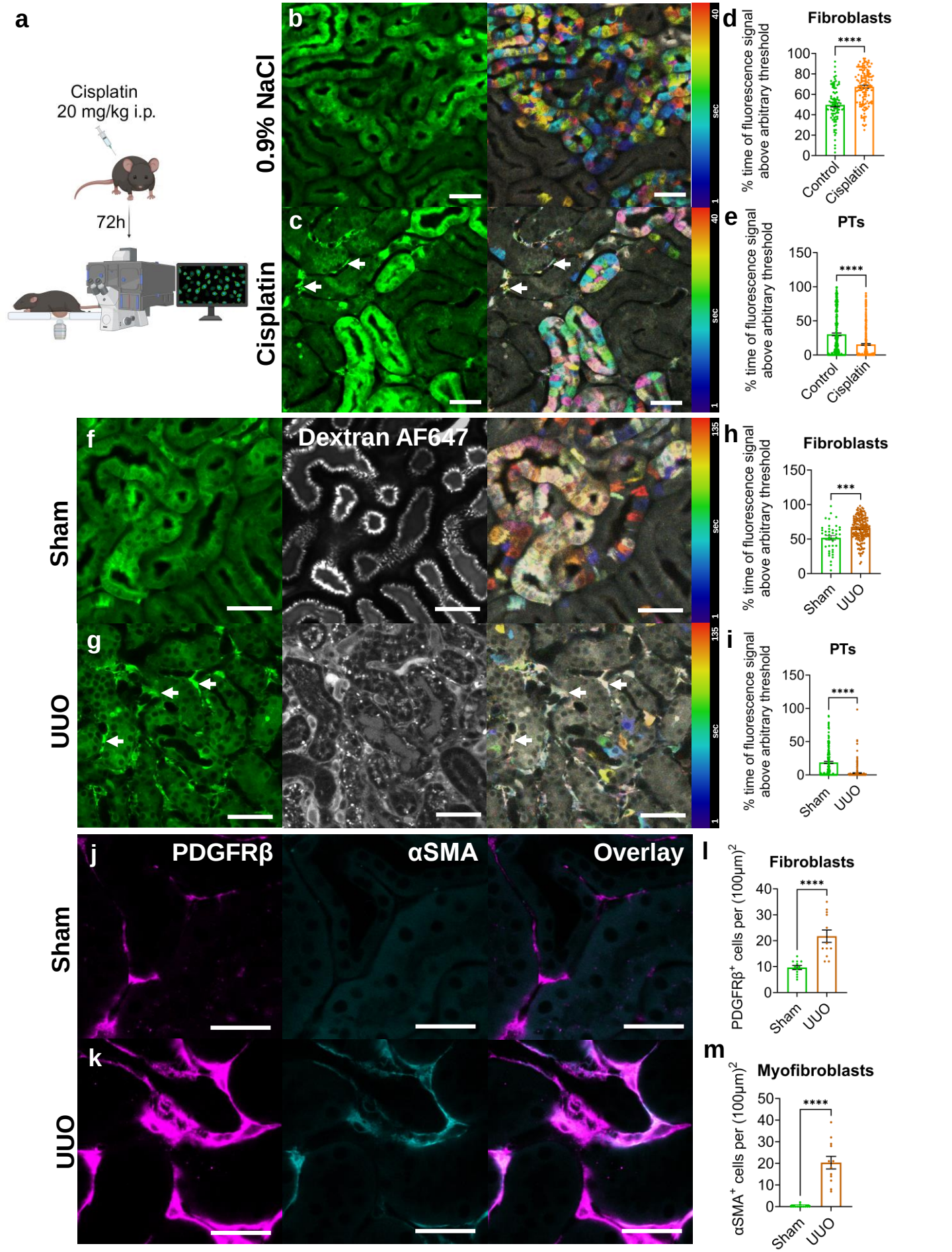
a
Cisplatin
20 mg/kg i.p.
72h
0.9% NaCl
Cisplatin
b
c
d
Fibroblasts
% time of fluorescence signal above arbitrary threshold
Control
Cisplatin
e
PTs
f
Dextran AF647
Sham
g
UUO
h
Fibroblasts
Sham
UUO
i
PTs
j
PDGFRβ
αSMA
Overlay
k
l
Fibroblasts
PDGFRβ+ cells per (100μm)2
m
Myofibroblasts
αSMA+ cells per (100μm)2

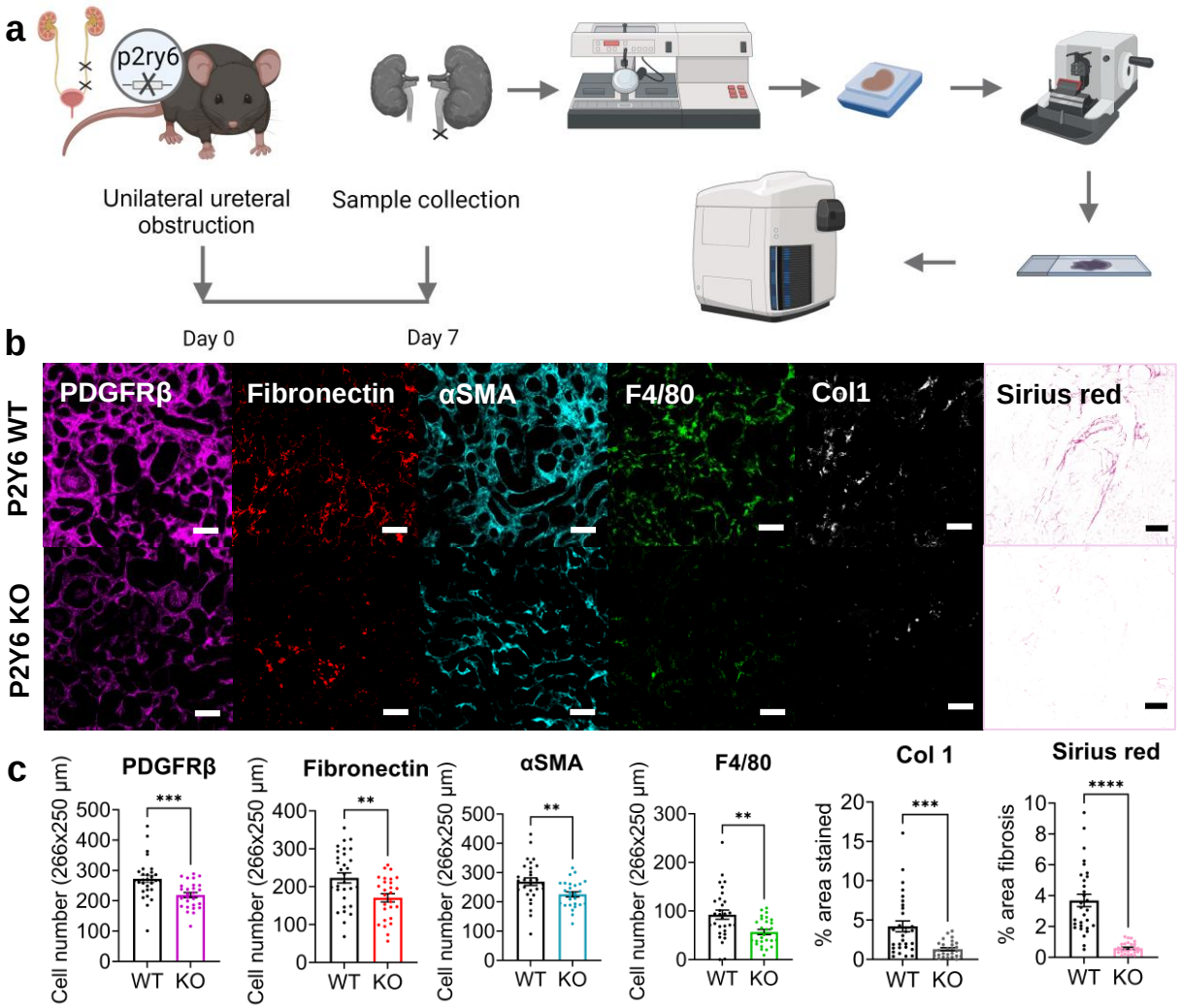
a
p2ry6
Unilateral ureteral obstruction
Sample collection
Day 0
Day 7
b
P2Y6 WT
P2Y6 KO
PDGFRβ
Fibronectin
αSMA
F4/80
Col1
Sirius red
c
PDGFRβ
Fibronectin
αSMA
F4/80
Col 1
Sirius red
Cell number (266x250 µm)
% area stained
% area fibrosis
WT
KO
***
**
****

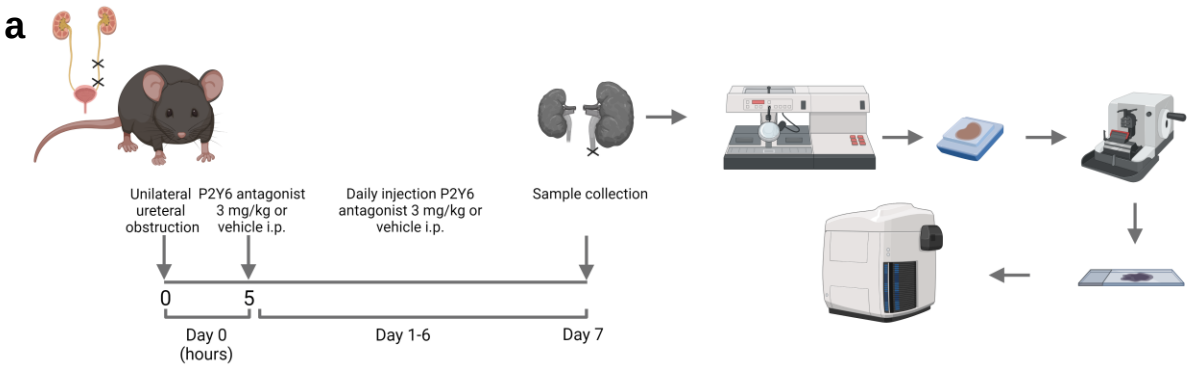
a
Unilateral ureteral obstruction
P2Y6 antagonist 3 mg/kg or vehicle i.p.
Daily injection P2Y6 antagonist 3 mg/kg or vehicle i.p.
Sample collection
0
5
Day 0 (hours)
Day 1-6
Day 7

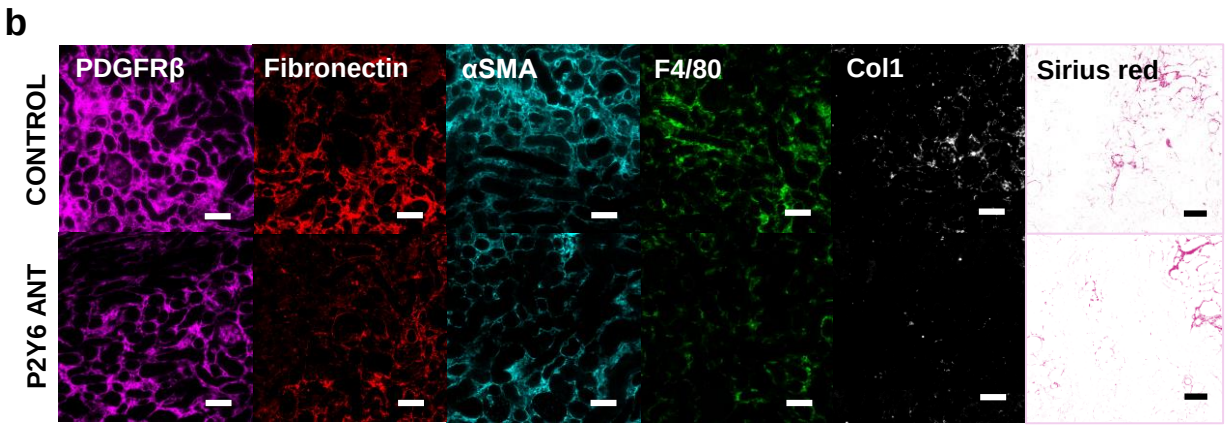
b
CONTROL
P2Y6 ANT
PDGFRβ
Fibronectin
αSMA
F4/80
Col1
Sirius red

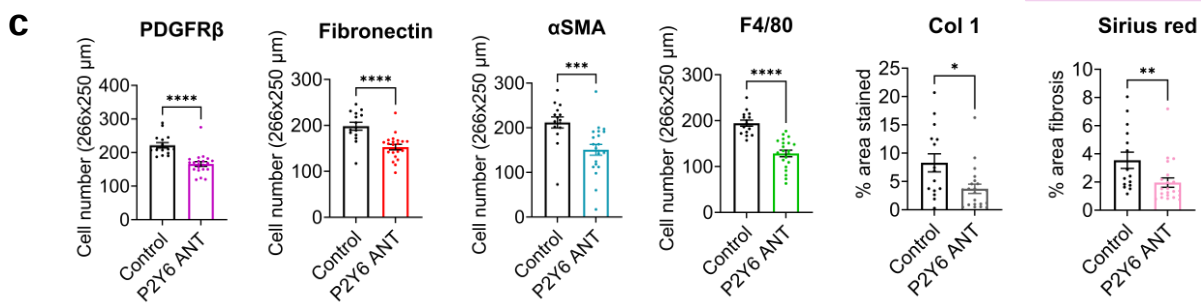
c
PDGFRβ
Fibronectin
αSMA
F4/80
Col 1
Sirius red
Cell number (266x250 µm)
% area stained
% area fibrosis
Control
P2Y6 ANT
****
***
**
*

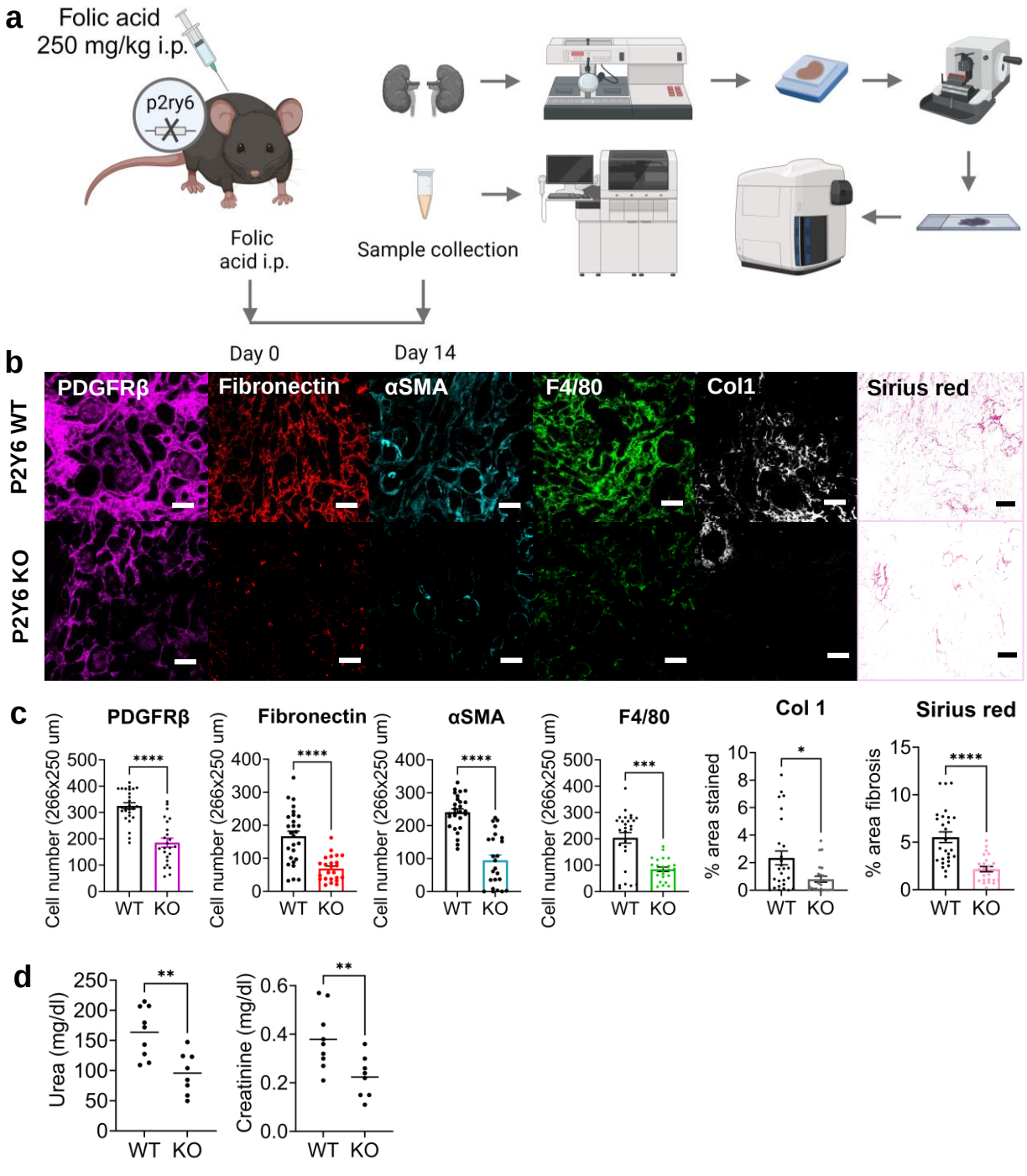
a
Folic acid
250 mg/kg i.p.
p2ry6
Folic
acid i.p.
Sample collection
Day 0
Day 14
b
PDGFRβ
Fibronectin
αSMA
F4/80
Col1
Sirius red
P2Y6 WT
P2Y6 KO
c
PDGFRβ
Fibronectin
αSMA
F4/80
Col 1
Sirius red
Cell number (266x250 um)
% area stained
% area fibrosis
WT
KO
****
***
*
d
Urea (mg/dl)
Creatinine (mg/dl)
**

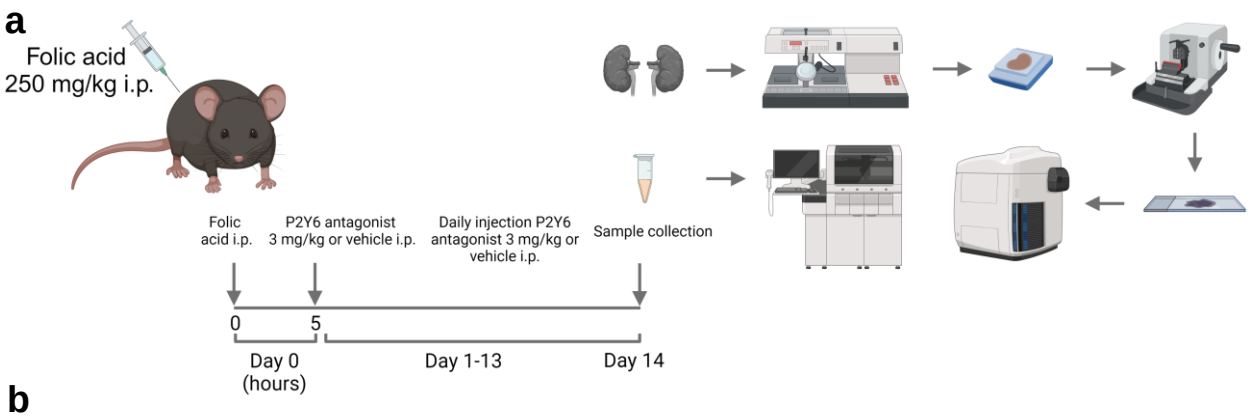
a
Folic acid
250 mg/kg i.p.
Folic acid i.p.
P2Y6 antagonist 3 mg/kg or vehicle i.p.
Daily injection P2Y6 antagonist 3 mg/kg or vehicle i.p.
Sample collection
0
5
Day 0 (hours)
Day 1-13
Day 14

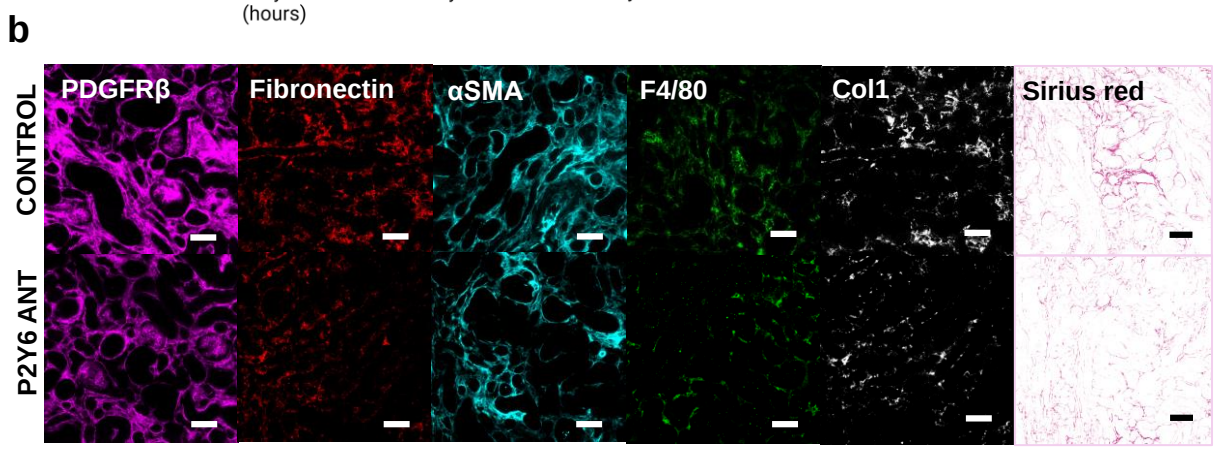
b
CONTROL
P2Y6 ANT
PDGFRβ
Fibronectin
αSMA
F4/80
Col1
Sirius red

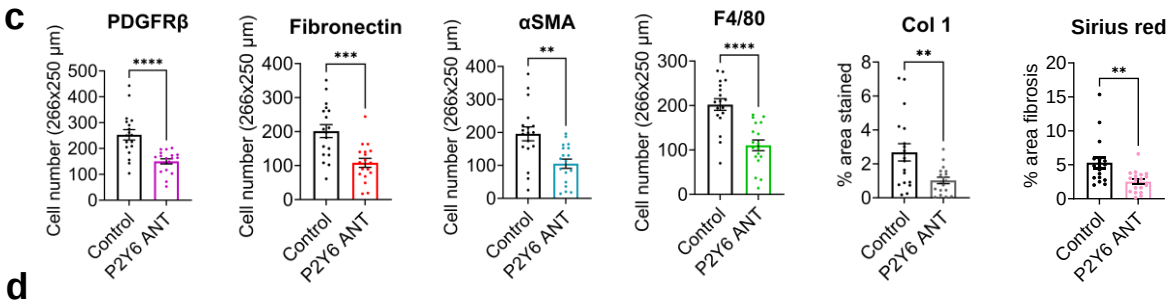
c
PDGFRβ
Cell number (266x250 µm)
****
Fibronectin
***
αSMA
**
F4/80
****
Col 1
% area stained
**
Sirius red
% area fibrosis
**
Control
P2Y6 ANT

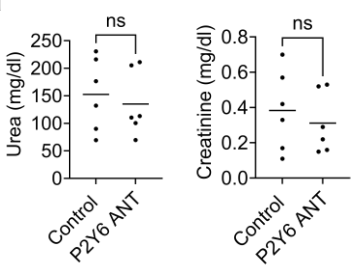
d
Urea (mg/dl)
ns
Creatinine (mg/dl)
ns
Control
P2Y6 ANT

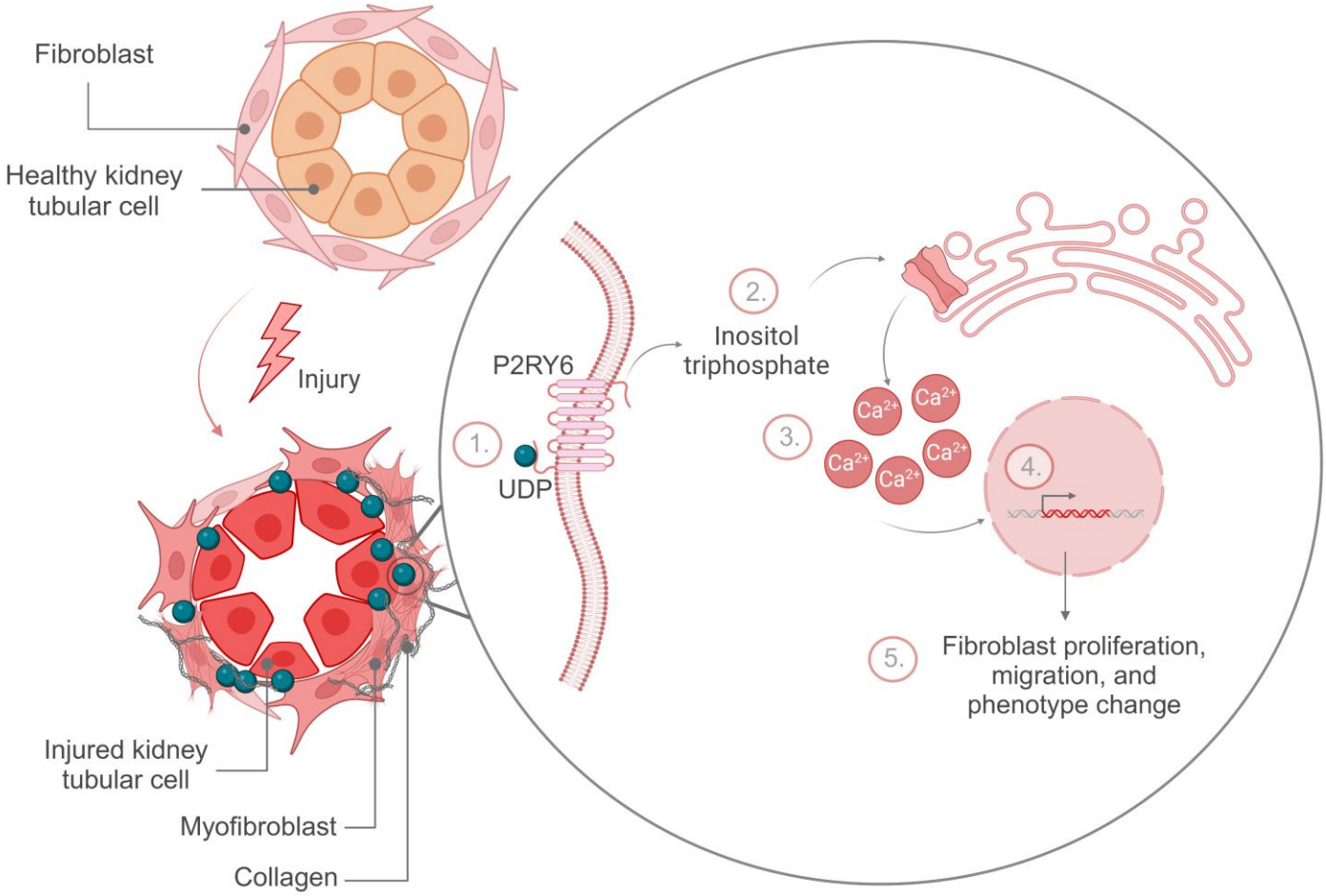
Fibroblast
Healthy kidney tubular cell
Injury
Injured kidney tubular cell
Myofibroblast
Collagen
P2RY6
1.
UDP
2.
Inositol triphosphate
3.
Ca2+
4.
5.
Fibroblast proliferation, migration, and phenotype change